Journal Pre-proofs

Research paper

Immunogenicity of a silica nanoparticle-based SARS-CoV-2 vaccine in mice

Clara Barbey, Jinpeng Su, Martina Billmeier, Nadine Stefan, Romina Bester, George Carnell, Nigel Temperton, Jonathan Heeney, Ulrike Protzer, Miriam Breunig, Ralf Wagner, David Peterhoff

PII: S0939-6411(23)00258-8
DOI: https://doi.org/10.1016/j.ejpb.2023.09.015
Reference: EJPB 14110

To appear in: *European Journal of Pharmaceutics and Biopharmaceutics*

Received Date: 28 June 2023
Revised Date: 12 September 2023
Accepted Date: 26 September 2023

Please cite this article as: C. Barbey, J. Su, M. Billmeier, N. Stefan, R. Bester, G. Carnell, N. Temperton, J. Heeney, U. Protzer, M. Breunig, R. Wagner, D. Peterhoff, Immunogenicity of a silica nanoparticle-based SARS-CoV-2 vaccine in mice, *European Journal of Pharmaceutics and Biopharmaceutics* (2023), doi: https://doi.org/10.1016/j.ejpb.2023.09.015

Immunogenicity of a silica nanoparticle-based SARS-CoV-2 vaccine in mice

Clara Barbey[1]*, Jinpeng Su[2]*, Martina Billmeier[3], Nadine Stefan[3], Romina Bester[2], George Carnell[4], Nigel Temperton[5], Jonathan Heeney[4], Ulrike Protzer[2,6], Miriam Breunig[1], Ralf Wagner[3,7,Δ], and David Peterhoff[3,7,Δ,†]

* / Δ equal contribution

† corresponding author (david.peterhoff@ur.de)

1 Department of Pharmaceutical Technology, University of Regensburg, Regensburg, Germany

2 Institute of Virology, Technical University of Munich / Helmholtz Munich, Munich, Germany

3 Institute of Medical Microbiology and Hygiene, University of Regensburg, Regensburg, Germany

4 Lab of Viral Zoonotics, Department of Veterinary Medicine, University of Cambridge, Cambridge, United Kingdom

5 Viral Pseudotype Unit, Medway School of Pharmacy, The Universities of Greenwich and Kent at Medway, Chatham ME4 4BF, United Kingdom

6 German Center for Infection Research (DZIF), Munich partner site, Germany

7 Institute of Clinical Microbiology and Hygiene, University Hospital Regensburg, Regensburg, Germany

Abstract

Safe and effective vaccines have been regarded early on as critical in combating the COVID-19 pandemic. Among the deployed vaccine platforms, subunit vaccines have a particularly good safety profile but may suffer from a lower immunogenicity compared to mRNA based or viral vector vaccines. In fact, this phenomenon has also been observed for SARS-CoV-2 subunit vaccines comprising the receptor-binding domain (RBD) of the spike (S) protein. Therefore, RBD-based vaccines have to rely on additional measures to enhance the immune response. It is well accepted that displaying antigens on nanoparticles can improve the quantity and quality of vaccine-mediated both humoral and cell-mediated immune responses. Based on this, we hypothesized that SARS-CoV-2 RBD as immunogen would benefit from being presented to the immune system via silica nanoparticles (SiNP). Herein we describe the preparation, *in vitro* characterization, antigenicity and *in vivo* immunogenicity of SiNPs decorated with properly oriented RBD in mice.

We found our RBD-SiNP conjugates show narrow, homogeneous particle distribution with optimal size of about 100 nm for efficient transport to and into the lymph node. The colloidal stability and binding of the antigen was stable for at least 4 months at storage- and *in vivo*-temperatures. The antigenicity of the RBD was maintained upon binding to the SiNP surface, and the receptor-binding motif was readily accessible due to the spatial orientation of the RBD. The particles were efficiently taken up *in vitro* by antigen-presenting cells. In a mouse immunization study using an mRNA vaccine and spike protein as benchmarks, we found that the SiNP formulation was able to elicit a stronger RBD-specific humoral response compared to the soluble protein. For the adjuvanted RBD-SiNP we found strong S-specific multifunctional $CD4^+$ T cell responses, a balanced T helper response, improved auto- and heterologous virus neutralization capacity, and increased serum avidity, suggesting increased affinity maturation.

In summary, our results provide further evidence for the possibility of optimizing the cellular and humoral immune response through antigen presentation on SiNP.

Graphical Abstract

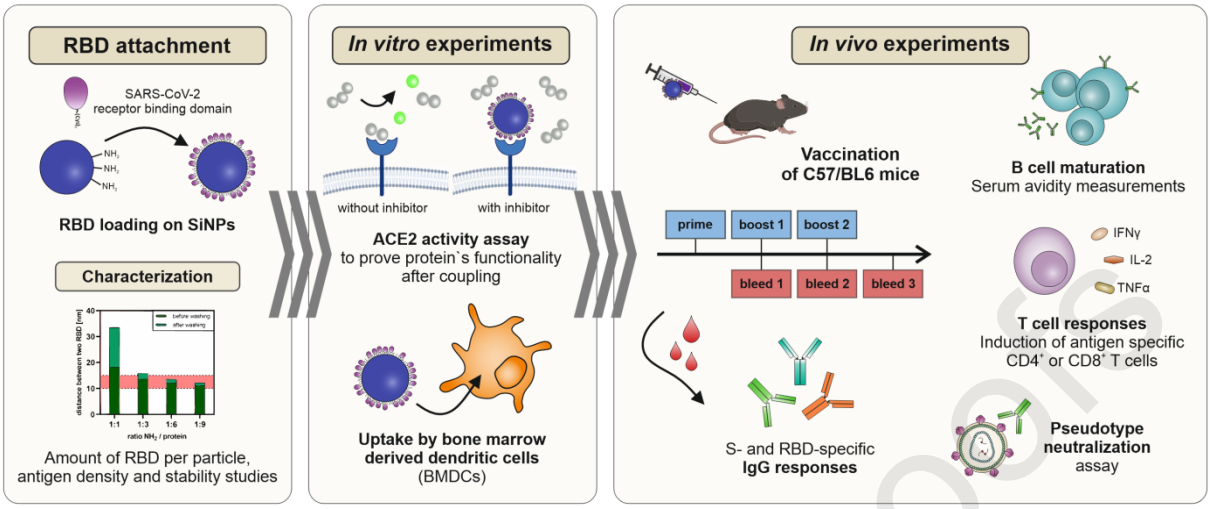

1. Introduction

Vaccines against severe acute respiratory syndrome coronavirus 2 (SARS-CoV-2) have played a central role in combating the coronavirus disease 2019 (COVID-19) pandemic. Evidence for the protective potential of virus-neutralizing antibodies from other viral infectious diseases led to an early focus on their main target in SARS-CoV-2, the viral spike (S) protein and its receptor-binding domain (RBD). In fact, the sole antigen that was part of all four vaccine-platforms with emergency approval (mRNA, inactivated virus, adenoviral vector, and protein subunit) was the S protein or variants thereof and neutralizing antibodies were important endpoints of the associated clinical trials. Antibody specificities overlapping with the receptor-binding motif (RBM) of the cellular receptor Angiotensin-converting enzyme 2 (ACE2) should competitively inhibit infection. Thus the idea of RBD-based vaccines – which should elicit such antibodies – initially seemed particularly promising. Furthermore, such focusing of the antibody response to relevant epitopes would avoid the induction of putatively infection-enhancing antibodies simultaneously [1]. However, evidence from preclinical and early clinical studies suggested superior immunogenicity and safety profiles of prefusion-stabilized spike vaccines compared to RBD candidates and therefore in many cases led to its deprioritization [2–6]. Nevertheless, some recent clinical trials are investigating the advantages of a well-designed RBD-based immunogen and its optimal formulation and some have provided encouraging results [7].

In the context of comparable modern protein subunit vaccines that focus the immune response on specific epitopes, the use of nanoparticles has gained increasing importance as they can strongly enhance an intrinsically low humoral response [8–10]. The multivalent presentation of an antigen offers several advantages: (i) it mimics the natural pathogen structure [11–13], (ii) supports the activation of low-affinity reactive naïve B cells [14], (iii) facilitates transport to the lymph node by professional antigen-presenting cells (APCs) [11–15], (iv) enhances uptake of the antigen into APCs [16], enabling subsequent presentation of its peptides, (v) generates antigen depots [17], and (vi) provides intrinsic adjuvant properties [18]. A number of preclinical studies have recently shown significantly improved potency and breadth of induced antibody (Ab) serum levels by nanoparticle delivery of antigens e.g. from HIV-1 [19], respiratory syncytial virus [20], influenza [21], *P. falciparum* [22], Hepatitis B virus [23], and Dengue virus [24] . A variety of nanoparticle platforms have been established and it

has gained recognition that parameters such as size, particle stability, spatial arrangement and stability of antigen binding, immunogenicity of the nanoparticle carrier, toxicity and biodegradability need to be considered in the development of such platforms [13,14]. In this context, the specific advantages of silica nanoparticles (SiNPs) as a vaccine platform have been demonstrated and suitable techniques haven been developed to functionalize both the particle and the antigen for efficient coupling [25–28].

Here, we used SiNPs for the presentation of the SARS-CoV-2 S RBD protein. For optimal presentation of the antigen on the SiNP surface, we coupled via a site-specific and oriented covalent conjugation, which was already proven efficient for other viral immunogens [27,28]. For this purpose, we fused the antigen with a tandem cysteine tag at the N-terminus (NtCC) to couple it to maleimide-functionalized SiNPs. The resulting RBD-SiNPs were characterized regarding the amount and density of RBD on their surface, the colloidal stability and the attachment stability. Protein integrity after coupling and the antigenic profile of the RBD were characterized by analysis of binding antibodies and an *in vitro* ACE2 inhibition assay. Furthermore, the recognition and the uptake by bone marrow dendritic cells (BMDCs) was evaluated *in vitro.* Finally, the immunogenicity of the RBD-SiNPs was tested *in vivo* in mice, which proved the advantages of the nanoparticulate delivery regarding both humoral and cellular immune response, neutralization capacity and avidity.

2. Material and Methods

2.1. Materials

All used chemicals were supplied from Sigma Aldrich (Taufkirchen, Germany) unless otherwise stated. Non-porous 100 nm silica nanoparticles (sicastar white and sicastar greenF suspension*)* with an amino functionalized surface (1 µmol NH_2/g) were purchased from micromod (Rostock, Germany). Ultrapure water was generated by a Milli-Q water purification system (Merck Millipore, Germany). Tibias and femurs of male C57BL/6J mice were kindly provided by Prof. Dr. Dr. André Gessner (Institute of Medical Microbiology and Hygiene, University Regensburg).

2.2. Protein expression and purification

The SARS-CoV RBDs were cloned, expressed and purified essentially as described earlier [29,30]. Briefly, pcDNA5/FRT/TO vector-based constructs, which included an N-terminal cysteine-containing tag (NtCC, [27]) and a C-terminal avi-hexahistidine tag [31], were transiently transfected into Expi293F cells (Thermo Fisher Scientific; A14527) and after 5 days of protein expression, supernatants were harvested by centrifugation, purified by immobilized metal chelate affinity chromatography (IMAC).

The SARS-CoV-2 D614G stabilized spike ectodomain (S-trimer) was expressed and purified as described earlier [29]. Here in addition to IMAC a subsequent size exclusion chromatography (SEC) was used to generate homogeneous trimeric protein.

Construct generation and purification of the monoclonal antibodies and soluble ACE2 (amino acid 20–732) used in this study was described earlier by Mader *et al.* [30]. The constructs were transiently transfected and expressed in Expi293F cells and purified from the supernatants. Antibodies were purified by protein A affinity purification. Soluble ACE2 was purified by IMAC and subsequent anion exchange chromatography.

All proteins were buffer exchanged to PBS and stored at 4 °C.

2.3. Biochemical characterization of the soluble proteins

2.3.1 Immunosorbent Assay (ELISA)

ELISA was performed as described recently [30]. Briefly, 100 ng RBD per well was coated in a 96-well Nunc Maxisorp ELISA plate (Thermo Fisher Scientific). The plate was blocked with 5% fat free milk powder in phosphate-buffered saline with 0.1% Tween-20 (PBS-T), washed with PBS-T and antibody was added in PBS-T containing

1% fat free milk powder. After washing, peroxidase-conjugated polyclonal rabbit anti-human IgG (Dako) was added. Plates were developed by adding 3,3′,5,5′-Tetramethylbenzidin (TMB) substrate and the reaction was stopped by adding 2 N sulfuric acid. Optical density (OD) at 450 nm (subtraction of background absorption at 630 nm) was measured in an ELISA plate reader (Microplate Reader Model 680, Bio-Rad).

2.3.2 Sodium dodecyl sulfate polyacrylamide gel electrophoresis (SDS-PAGE)

Samples were applied in Laemmli sample buffer and loaded on a precast gradient SDS-PAGE (SERVAGel TG Prime 8-16% polyacrylamide). After electrophoresis, the gel was stained with Coomassie and imaged a gel documentation system (ChemiDoc, Bio-Rad).

2.3.3 Analytical size exclusion chromatography (SEC)

Analytical SEC was conducted on a Superdex 200 Increase size exclusion column (Cytiva, USA) operated on an Agilent 1100 series HPLC (Agilent). The chromatography was performed in PBS at a flow rate of 0.75 mL/min at room temperature and a total volume of 25 µL of a 1.0 mg/mL protein solution was loaded per run.

2.4. Site specific biotinylation and labelling of proteins

Site specific biotinylation at the avi-tag was performed using the BirA enzyme system. BirA biotin-protein ligase standard reaction kit (Avidity LLC, Colorado, USA) was used for the biotinylation according to the manufacturer's recommendation.

Labelling of proteins and antibodies (ACE2, CR3022 and S309) with the fluorescent dye Alexa Fluor 647 (AF647) was performed using the AF647 labelling kit from Thermo Fisher Scientific (A20186).

2.5. Immobilization of RBD proteins to SiNPs

As platform for immobilization of SARS-CoV-2 RBD proteins, 100 nm amino functionalized SiNPs were used. The particles were diluted to a final concentration of 10 mg/ml in millipore water. In a first step, sulfosuccinimidyl 4-(N-maleimidomethyl) cyclohexan-1-carboxylat (sulfo-SMCC), as a sulfhydryl- and amine- reactive heterobifunctional linker, was incubated in a 50-fold molar excess to the available NH_2-groups on the SiNPs under gently shaking for one hour at room temperature. The

particles were washed twice with millipore water via centrifugation (9,000 rcf, 9 min, 4 °C) to remove the excess of sulfo-SMCC linker. Before adding the protein in 3-fold molar excess to the particles, the RBD with a cysteine tag on the N-terminus was reduced with 0.5 mM tris-(2-carboxyethyl)-phosphine (TCEP), and the mixture was incubated overnight at room temperature. To remove excess protein, RBD-SiNPs were washed twice with fresh millipore water and centrifugation (9,000 rcf, 9 min, 4 °C). The pellet was resuspended in 100 mM arginine in millipore water. RBD-SiNPs were stored at 4 °C. Finally, to remove tightly adsorbed protein, a second washing step was performed using PBS supplemented with 1% (v/v) Tween20 by centrifugation (9,000 rcf, 9 min, 4 °C).

2.6. Characterization of RBD-SiNP

2.6.1 Dynamic light scattering

The hydrodynamic diameter and the polydispersity index (PDI) of the blank SiNPs and RBD-SiNPs were measured using a Zetasizer Nano ZEN 3600 (Malvern Instruments, Worcestershire, United Kingdom). The refractive index for the silica was adjusted to 1.45 and the SiNP concentration was diluted to 0.5 mg/ml. All size measurements were performed in millipore water. All results were analyzed by Malvern Zetasizer Software version 7.11 (Malvern Instruments, Worcestershire, United Kingdom).

2.6.2 Determination of protein amount on the SiNPs

A QuantiPro™ BCA Assay Kit was used to define the amount of conjugated RBD proteins to the surface of SiNPs. The calibration curve was performed with soluble RBD in a range between 0.1 and 70 µg/ml. According to manufacturer's instructions, standards (n=3) and samples (n=4) were mixed with copper (II)-sulfate-containing working reagent and were incubated at 60 °C for one hour. Afterwards, the absorbance at 562 nm was read with a plate reader (Fluostar Omega, BMG Labtech, Ortenberg, Germany). In order to calculate the protein amount, the measured absorbance of the blank SiNPs was subtracted from the absorbance of the conjugates. The absolute number of RBD molecules per particle was calculated from converting the protein concentration of the samples into the total number of RBD proteins based on the molecular weight (MW_{RBD} = 27 kDa) and the Avogadro constant ($N_A = 6.022 \cdot 10^{23}$ mol^{-1}) in comparison to the number of initially applied particle concentration and the total number of particles per mg provided by the manufacturer ($9.5 \cdot 10^{11}$ particles/mg). This

BCA assay was performed after the first and the second washing step to determine the tightly adsorbed protein.

2.6.3 Protein release assay

RBD-SiNPs were incubated in 100 mM arginine at 4 °C and 37 °C. The samples were centrifuged (9,000 rcf, 9 min, 4 °C) at defined time points and the protein amount in the supernatant was quantified via QuantiPro™ BCA assay kit. The particle pellets were re-suspended in fresh 100 mM arginine in millipore water. This procedure was repeated at multiple time points over a period of 120 days.

2.6.4 Colloidal stability test

The hydrodynamic diameter and the PDI as indication of the colloidal stability were measured at predefined time points using dynamic light scattering (DLS). To this end, RBD-SiNP were incubated in 100 mM arginine in millipore water at 4 °C and 37 °C over 120 days.

2.7. Protein integrity after coupling

2.7.1 Microscale thermophoresis for binding studies

Microscale thermophoresis (MST) was used to measure the binding of ACE2 and the antibodies CR3022 and S309 to the RBD-SiNPs in comparison to soluble RBD. As negative control human serum albumin (HSA) blocked SiNPs were analyzed to control unspecific binding. The experiment was conducted in PBS supplemented with 0.05% Polysorbate 20. The antibodies and the ACE2 protein were fluorescently labeled with AF647 according to protocol and the concentration of protein or antibody was adjusted to 1 nM. Sixteen 2-fold serial dilutions of the RBD-SiNPs and the unbound RBD starting from a protein concentration of 400 nM were added to an equal volume of labeled protein or antibody. These mixtures were incubated for 15 minutes at room temperature and were measured in standard capillaries (Monolith NT 155). The MST measurements were performed with 15% to 17% excitation power and 80% MST power using a Monolith NT p115 MST device (Nanotemper Technologies, Munich, Germany). Binding curves and K_d values were analyzed with MO. Affinity Analysis Software version 2.1.1 (Nanotemper Technologies, Munich, Germany).

2.7.2 ACE2 activity competition assay

HEK 293T cells stably expressing ACE2 (HEK-293T-ACE2) were cultivated and prepared at 12,000 cells per well. RBD-SiNPs and HSA coated SiNPs were pipetted in a final protein concentration of 10, 50 and 100 nM (n=3 each) to the cells and resulting mixtures were incubated for one hour at 37 °C. After incubation, the cells were lysed, the samples were centrifuged (16,000 rcf, 4 °C, 10 min) and the supernatant was incubated with a fluorogenic ACE2 substrate (PromoKine ACE2 activation assay kit, PromoCell GmbH, Heidelberg, Germany) for 15 minutes at ambient temperature. The fluorescence intensity was measured at an emission wavelength of 420 nm over 60 minutes using a BioTek Synergy neo2 multi-mode reader (Agilent Technologies, Santa Clara, USA).

2.8. Confocal laser scanning microscopy (CLSM) analysis of *in vitro* uptake by BMDCs

BMDCs were cultivated and prepared according to a previously described protocol [32]. Briefly, bone marrow from tibias and femurs of male C75BL/6J mice 15 weeks old was collected and the obtained cell suspension was cultivated in 5 ng/ml GM-CSF (Pepro Tech, London, UK) containing RPMI 1640 (Biochrom GmbH, Berlin, Germany) at 37 °C and 5% CO_2. Three and six days after collection, fresh GM-CSF containing RPMI 1640 was added. BMDCs were harvested, washed and prepared for *in vitro* uptake experiments. On day seven, $0.1 \cdot 10^6$ BMDCs per well were seeded into an 8-well slide (ibidi, Planegg, Germany) for CLSM analysis. The BMDCs-loaded slides were cultivated for 5 h. Afterwards, conjugates with FITC labeled SiNPs and AF647-labelled RBDs were added in a final SiNP concentration of 0.5 mg/ml. The mixtures were cultivated for 16 h. Subsequently, the cell preparations were washed with PBS and covered with Leibovitz medium containing 10% FBS. All samples were analyzed with a LSM 510 Meta confocal microscope using an argon laser at 488 nm and a HeNe laser at 633 nm for excitation. The emitted light was detected after passing a band-pass filter of 505-530 nm and a long-pass filter of 630 nm. Images were analyzed by Zen blue software version 3.5 (Zeiss, Wetzlar, Germany).

2.9. Ethical statements and immunization protocol of mouse experiments

Animal experiments were conducted in strict accordance with the German regulations of the Society for Laboratory Animal Science (GV-SOLAS) and the European Health Law of the Federation of Laboratory Animal Science Associations (FELASA). Experiments were approved by the District Government of Upper Bavaria (permission

number: ROB-55.2-2532.Vet_02-20-193). Mice were kept in pathogen-free animal facilities following institutional guidelines. Ten weeks old wild-type C57BL/6J mice purchased from Janvier Labs (Le Genest-Saint-Isle, France) were immunized subcutaneously three times with 8 µg S-trimer, RBD, RBD-SiNP with 24 µg MPLA adjuvant, or 8 µg RBD-SiNP without adjuvant at week 0, 2, 4, respectively. Mice receiving PBS injections served as controls. For the mRNA vaccine group, mice were immunized intramuscularly with 5 µg of BNT162b2 mRNA vaccine (Tozinameran, BioNTech/Pfizer) at week 0 and 4. One week after the last immunization, the mice were sacrificed for the final analyses of vaccine-induced antibodies and T-cell responses.

2.10. Analysis of serum S- and RBD-specific IgG responses by ELISA

S- and RBD-specific IgG concentration was measured in mouse sera from the endpoint of experiment with a quantitative ELISA as described previously [33]. Briefly, ELISA plates were coated with 100 µl of 500 ng/ml S protein (SinoBiological, China) or RBD protein (SinoBiological, China) at 4 °C overnight. For the standard curve of quantitating IgG, the plates were coated with serial diluted mouse IgG protein (Sigma-Aldrich, Germany) starting with 500 ng/ml. After washing with PBS containing 0.05% Tween 20 (PBST), the wells were blocked with 200 µl of 5% FCS in PBS for 2 h at room temperature (RT). Diluted mouse sera (1:500 in PBS) were then added into the S protein or RBD coated wells. PBS was added into the IgG coated wells. After 2 h incubation at RT and washing, the wells were treated with 100 µl of horseradish peroxidase (HRP)-conjugated goat anti-mouse IgG antibody (Sigma-Aldrich, 1:2000 in PBS) for 1 h at RT. After five washing steps, 100 µl of stabilized chromogen TMB solution was added to each well. The plates were incubated in the dark for two to three minutes and the reaction was stopped by adding 100 µl of 2 N sulfuric acid per well. OD was determined at the wavelength of 450 nm (measurement) and 560 nm (background subtraction) employing a plate reader (Tecan Infinite F200, Tecan, Germany).

2.11. Analysis of serum RBD-specific IgG responses by Luminex

Luminex Binding Antibody Multiplex Assay was performed essentially as described earlier [34]. In brief, biotinylated antigens were captured to the MagPlexAvidin Microspheres (Luminex, Austin, TX, USA). After blocking, diluted sera were applied at

a 1:500 dilution. After washing, secondary antibodies were applied and detected by a MAGPIX instrument (Luminex, Austin, TX, USA).

R-Phycoerythrin conjugated secondary antibodies used included: Rat anti-mouse IgG_1 (Biolegend, San Diego, CA, USA), donkey anti-mouse IgG, goat anti-mouse IgG_{2b}, goat anti-mouse IgG_{2c} and goat anti-mouse IgG_3 (all from Jackson ImmunoResearch, West Grove, PA, USA). All conjugated secondary antibodies were used at a 1:200 dilution.

2.12. Isolation of murine splenocytes and intracellular cytokine staining

Murine splenocytes were isolated as described previously [35]. Briefly, spleens were mashed through a 100 µm cell strainer, and erythrocytes were lysed by incubating the cells with ammonium-chloride-potassium (ACK) lysis buffer for one minute at RT. For estimation of intracellular production of the cytokines, first, splenocytes were stimulated with 1 µg/ml of PepMix SARS-CoV-2 S pool 1 or S pool 2 (JPT, Germany) in the presence of brefeldin A (BFA) overnight. Cells stimulated with ovalbumin-derived peptide (OVAS8L, SIINFEKL) served as negative controls. On the following day, cell surface staining was performed using anti-CD4, anti-CD8 antibodies. Dead cells were excluded from analysis by Fixable Viability Dye eF780 (eBioscience, Germany) staining. Intracellular cytokine staining of IFNγ, TNFα, IL-2 was performed as described [36]. Data were acquired on a CytoFlexS flow cytometer (Beckmann Coulter, USA) and analyzed using FlowJo software (Tree Star, USA).

2.13. T_h1/T_h2 cytokine secretion by stimulation of murine splenocytes

Up to $2 \cdot 10^6$ freshly isolated splenocytes per well were seeded into flat-bottom 96-well plates. For the stimulation, 2 µg/ml of S protein were added to the cells in a final volume of 300 µl per well. After 48-hour incubation at 37 °C, the supernatants were harvested to determine the concentration of secreted IFNγ, IL-4 and IL-5 by commercial ELISA kits (Invitrogen, USA), according to the manufacturer's instructions.

2.14. Pseudotype neutralization assay

2.14.1 Cultivation of adherent cell lines

HEK-293T/17 (ATCC) were cultured and maintained in Dulbecco's MEM (DMEM) supplemented with 10% Fetal Calf Serum (FCS) and 1% Penicillin/Streptomycin

(DMEM-K) at 37 °C and 5% CO_2 in a humidified incubator. HEK-293T-ACE2 cells [37] were grown in DMEM-K supplemented with 1 µg/mL puromycin.

2.14.2 Production of lentiviral pseudotypes and titration

The generation of lentiviral pseudotypes was carried out by transient transfection of HEK-293T/17 cells with the packaging plasmid p8.91 [38,39], the luciferase reporter plasmid pCSFLW and the desired amount of different SARS CoV-2 S expression plasmids (Wuhan D614G, VoC Delta, VoC Omicron sublineage BA.1) using the transfection reagent polyethyleneimine (PEI) as described previously [40]. Supernatants were harvested after 48 h, centrifuged at 2000 rcf for 5 min to remove cellular debris and stored at -80 °C until further use. Lentiviral pseudotypes were titrated on HEK-293T-ACE2 in a 2-fold serial dilution series using white 384-well culture plates. The luminescence was measured after 48 h by adding Bright-Glo (Promega) to each well and the signal (in relative light units, rlu) was read after a five-minute incubation period in a luminometer (Viktor^3, PerkinElmer) at 25 °C.

2.14.3 Lentiviral pseudotype based microneutralisation assay

The pseudotype-based microneutralisation assay was performed as described previously [41]. In brief, mouse sera were diluted in a 2-fold serial dilutions in DMEM-K in white 384-well culture plates. Lentiviral pseudotypes were added to serum dilutions and respective controls ($2.5{\cdot}10^5$ rlu/well) and incubated for 1 h at 37 °C. After 1 h $8{,}5{\cdot}10^4$ HEK-293T-ACE2 cells were added per well. After 48 h at 37 °C Bright-Glo was added to each well and the luminescence read out was carried in the luminometer after a 5 min incubation period. Half-maximal inhibitory concentrations (IC_{50}) were calculated after normalizing the data to the signals from uninfected (equivalent 100% neutralization) and infected (equivalent 0% neutralization) cells.

2.15. Statistical analyses

The statistical analyses and curve fittings were performed with GraphPad Prism (GraphPad Software Inc., San Diego, CA, USA). *P*-values <0.05 were considered significant.

3. Results

3.1. RBD preparation and characterization

To allow for efficient and site directed coupling of the RBD, we introduced an N-terminal cysteine tag (NtCC), which was described recently [27]. The tag contains two cysteines, which avoids disturbing the disulfide bridge architecture upon expression of the protein in mammalian cell culture. The cysteines are solvent accessible and can be used for site-specific coupling to the nanoparticles after reduction. In a previous work, the NtCC-tag was shown to greatly improve the coupling efficiency of HIV trimers to SiNPs via a heterobifunctional crosslinker using maleimide chemistry compared to a single C-terminal cysteine [27]. Likewise, in the case of RBD, we assume coupling primarily via the NtCC-tag, since the intrinsic 8 cysteine residues are buried inside the protein and form disulfide bridges there in the folded state of the protein.

To analyze the purity of the protein preparation we performed an SDS-PAGE (**Figure S1A**). To determine the influence of the N-terminal tag as well as the mild reduction with 0.5 mM TCEP on the structural integrity of the protein, we performed analytical SEC and an ELISA using the monoclonal antibodies CR3022, S309, and soluble ACE2. No significant differences of the structural and antigenic properties were observed in the SEC (**Figure S1B**) and ELISA experiment (**Figure S2**). Thus, a well-folded structure of the NtCC-RBD variant can be assumed even under mildly reducing coupling conditions.

3.2. RBD-SiNP preparation and characterization

After coupling of the antigen to 100 nm SiNPs, the particles passed either one or two washing steps (**Figure S3**). The first washing step was intended to remove excess protein ligand and loosely adsorbed protein. An additional second washing step was performed to remove tightly adsorbed protein from the nanoparticle surface (**Figure S3B**). In order to determine the reaction conditions that lead to homogeneous particle preparations and to achieve an antigen density on the particle surface that allows optimal activation of B cells, the coupling was carried out at different ratios of available NH_2-groups (or maleimide groups of the coupled crosslinker) on the SiNP surface to applied RBD. Then, the hydrodynamic diameter and the PDI of unmodified SiNPs and the resulting RBD-SiNPs were determined before and after the second washing step by dynamic light scattering (**Figure 1A**).

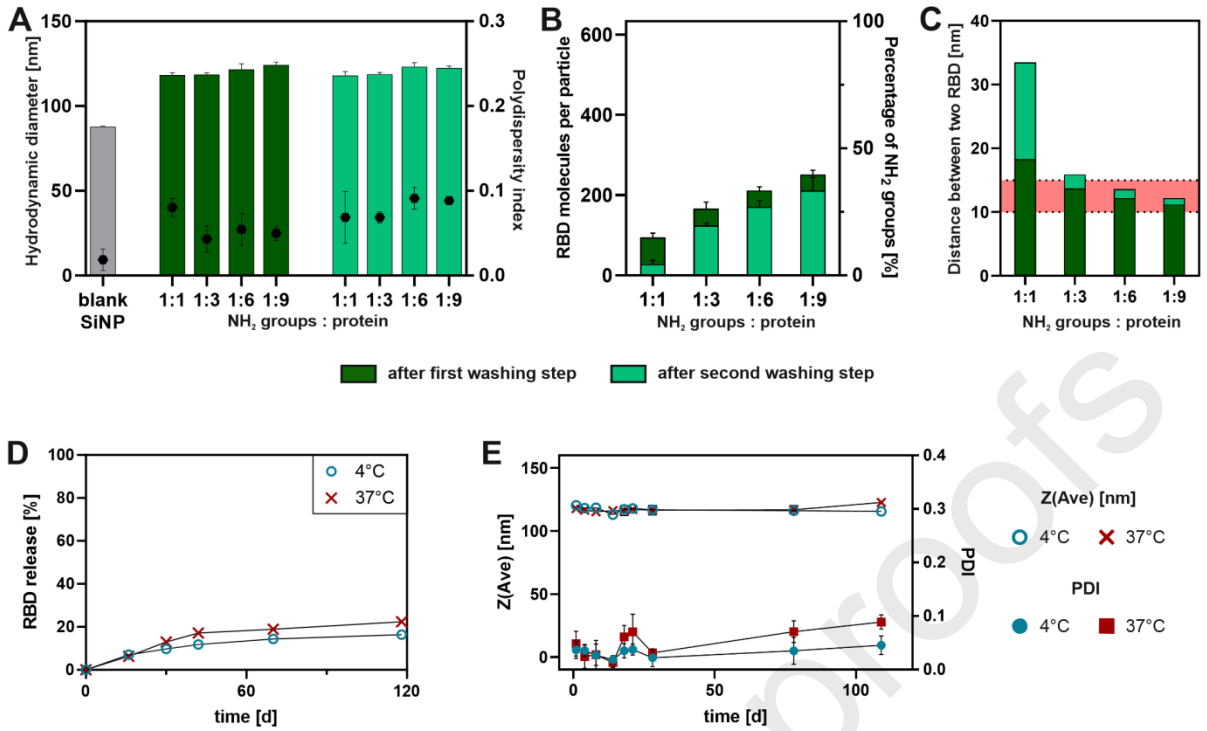

Figure 1: Characterization and stability studies of RBD-SiNPs synthesized with different ratios of available NH_2-groups per RBD used. Ratios were ranging from 1:1 up to 1:9. Hydrodynamic diameter shown as bars and the PDI shown as black squares of unmodified SiNPs and RBD-SiNPs before and after the second washing step were measured by DLS (A). Amount of attached RBD molecules to one particle after each washing step determined by BCA-Assay (B). Calculated center-to-center distances between two adjacent RBDs. The area highlighted in red between 10 nm and 15 nm shows the optimal distance between two proteins for increased antibody response (C). Result represents mean ± standard deviation (n=3). (D) Released RBD from RBD-SiNPs was measured in the supernatant by BCA assay over 120 days while incubating under storage conditions at 4 °C (blue circles) and at 37 °C (red crosses) (ratio 1:3, after the first washing step). At 4 °C 16% and at 37 °C 22% of the coupled RBD was released from the RBD-SiNP surface after 120 days. Results represent mean ± SD (n=3). (E) Colloidal stability of RBD-SiNPs over 120 days under storage conditions at 4 °C (blue circles) and at 37 °C (red crosses) (ratio 1:3, after the first washing step). Hydrodynamic diameter as indication of possibly occurring aggregation is shown as Z (Ave) on the left y-axis. No changes of the size occurred during longer incubation. For the PDI depicted as blue filled circles on the right side hardly any change was detected at 4 °C. A slight increase up to 0.09 was measured at 37 °C (red squares). Results represent mean ± SD (n=3).

The diameter of all RBD-SiNP preparations increased by about 35 nm compared to the unmodified SiNP resulting from adding the linker and the protein with its own hydrodynamic diameter. The PDI of all formulations was below 0.1. In addition, the amount of RBD on the SiNP surface after the first and the second washing step was determined by BCA assay and converted to the number of RBD molecules per SiNPs. With increasing ratio of NH_2-groups to RBD, the number of RBD molecules per SiNP

increased from 50 to 250 RBD molecules in linear relationship. This corresponds to an occupation of the available NH_2-groups ranging from about 15% to 40%. After removal of tightly adsorbed protein by the second washing step, a calculated amount of 30 to 210 RBD molecules remained on the surface of one particle, which corresponded to about 4% to 22% of the available NH_2-groups (**Figure 1B**). Assuming that the protein-ligands were evenly distributed on the nanoparticle surface, the center-to-center distance between two RBDs was calculated. As shown in **Figure 1C**, with increasing ratio of NH_2-groups to RBD, the distance between two RBD molecules decreased from about 18 nm to 11 nm. After the second washing step, the distances were slightly larger ranging from about 33 nm to 13 nm. The area highlighted in red shows the optimal distance between two proteins for optimized B cell receptor interaction [42].

Based on these experiments, we decided to use a 1:3 ratio of NH_2-groups per antigen and the two subsequent wash-steps for the preparation of the nanoparticles for the following experiments.

3.3. Attachment stability and colloidal stability

Attachment stability of the RBD to the SiNP surface is essential for long-term storage and *in vivo* functionality. We investigated the stability of RBD-SiNPs at 4 °C and 37 °C for 120 days. After 120 days, only 16% RBD was released into the supernatant at 4 °C and 22% at 37 °C, respectively (**Figure 1D**). Colloidal stability is equally important because agglomeration would impair the functionality of the conjugates. Similarly to the attachment stability, the colloidal stability of the RBD-SiNPs was investigated at 4 °C and 37 °C for 120 days. No substantial changes of the RBD-SiNP size occurred at both temperatures. While the PDI remained almost unchanged at 4 °C, a slight increase of the PDI up to 0.09 was detected at 37 °C **(Figure 1E**).

3.4. Structural integrity and epitope-accessibility of the SiNP surface-bound RBD

The accessibility of the RBM of the RBD is a prerequisite for the induction of competitively neutralizing antibodies. To test the accessibility of the RBM, binding to ACE-2 was measured by microscale thermophoresis (MST). Furthermore, to investigate differences in accessibility in epitopes located proximal to the coupling site (NtCC-tag) of the RBD, the binding of the two RBD-specific antibodies S309 and CR3022 was measured. **Figure 2C** illustrates the different angles of approach of the

antibodies and ACE2 with respect to the localization of the cysteine tag for covalent coupling to the SiNPs, and the SiNP-surface.

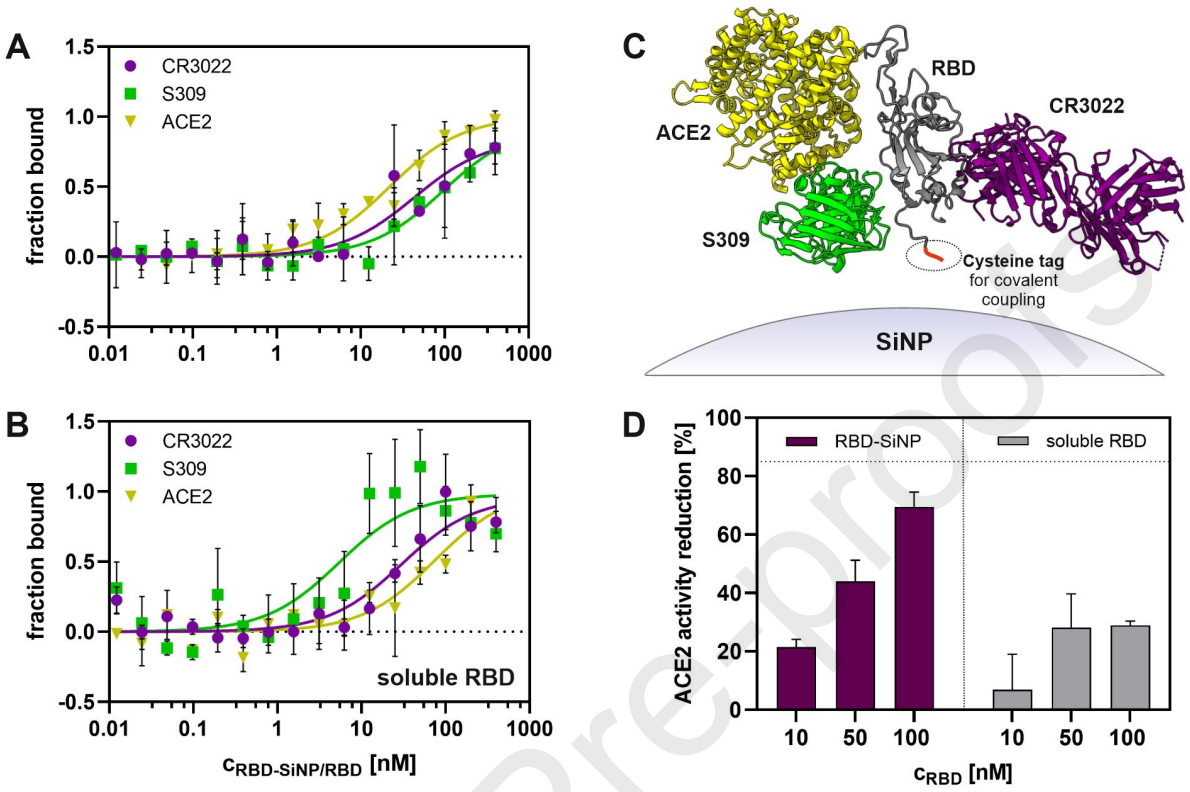

Figure 2: Differences in monoclonal antibody- and ACE2-binding of soluble and surface bound RBD, and detection of ACE2 binding of RBD by disturbing ACE2 activity. Protein structures illustrating the different angles of approach of the RBD ligands. Antibodies CR3022 (purple structure) S309 (green structure) and the soluble receptor ACE2 (yellow structure) to the RBD (grey structure) in relation to the localization of the cysteine tag (shown in red) are shown. MST binding curves of RBD-SiNP (A) and soluble RBD (B) to ACE2 (yellow triangles) and the neutralizing antibodies S309 (green square) and CR3022 (purple circles). HSA-SiNP were used as negative control to exclude non-specific binding (data not shown). Result represent mean ± SD (n=3). (D) The change of the fluorescence intensity caused by the conversion of the fluorogenic ACE2 substrate was measured in absence of RBD on membrane-bound ACE2 of HEK-293T-ACE2 cells. A reduced substrate conversion and therefore a reduced fluorescent signal is detected in the presence of soluble RBD or RBD-SiNP. ACE2 activity reduction in % of HEK-293T-ACE2 cells after treatment with RBD-SiNPs or soluble RBD is shown here as dark purple colored bars for RBD-SiNPs and as grey bars for the soluble RBD. RBD concentrations ranging from 10 to 100 nM were used. The fluorescence intensity of the conversion of the fluorogenic substrate caused by the residual ACE2 activity of HEK-293T-ACE2 cells was measured. The reduction of the ACE2 activity was calculated in relation to HSA covered SiNPs and soluble HSA as negative control. Result represent mean ± SD (n=3).

During MST measurements, the signals were normalized to fraction bound (0=unbound, 1=bound) as described previously [26]. The resulting binding curves of RBD-SiNPs and the soluble RBD to CR3022, S309 and ACE2 are shown in **Figure 2**.

All RBD-SiNP samples showed binding for all ligands, with ACE2 displaying higher affinity than CR3022 and S309 (**Figure 2A**). The binding studies were also performed with soluble RBD (**Figure 2B**). In contrast to the binding behavior of RBD-SiNP, the antibody S309 showed the highest binding affinity to the soluble RBD, followed by CR3022 and soluble ACE2.

From curve fits, apparent K_d values were calculated. Antibody CR3022 showed comparable apparent K_d values for RBD-SiNPs and soluble RBD with 43 nM and 30 nM, respectively (**Table S1**). In contrast, soluble RBD had a higher affinity to S309 (apparent K_d of 5 nM) compared to RBD-SiNPs (apparent K_d of 97 nM). RBD-SiNPs showed a higher affinity to ACE2 with an apparent K_d of 22 nM, whereas the soluble RBD bound with an apparent K_d of 74 nM. Blank SiNPs covered with human serum albumin (HSA) were used as negative control to exclude non-specific binding and showed no binding (data not shown).

3.5. ACE2-receptor binding capacity of the SiNP-bound RBD

As a further proof for structural integrity of the RBM in the RBD, an ACE2 activity competition assay was performed. In brief, the ACE2 receptor expressed on the surface of HEK-293T-ACE2 cells, allows for the conversion of a fluorogenic substrate. When RBD, either in its soluble form or bound to the SiNP surface, binds to ACE2, its enzymatic activity is blocked and conversion of the substrate is no longer possible. As negative control, HSA coated SiNPs and soluble HSA were investigated at the same protein concentrations as RBD-SiNPs and soluble RBD. RBD-SiNPs (dark purple bars) showed a concentration dependent ACE2 activity reduction from about 20% to 70% at a RBD concentration of 10 nM to 100 nM respectively. In contrast, the reduction caused by the soluble RBD (grey bars) was less pronounced (**Figure 2D**).

3.6. *In vitro* internalization of RBD-SiNP by BMDCs

One advantage of nanoparticulate antigen delivery is enhanced cellular uptake of particle-bound antigen. Efficient uptake of antigen is a prerequisite for the APC's contribution to the subsequent immune response. We tested this in murine BMDCs as a model for APCs, which were co-incubated for 16 h with either blank SiNPs, soluble RBD or RBD-SiNPs. CLSM analysis showed the internalization and thus the uptake of the blank particles, the soluble protein and the RBD-SiNPs by BMDCs (**Figure S4**). No

qualitative differences between the soluble RBD and the RBD-SiNPs were observed regarding RBD uptake.

3.7. Mouse immunization experiment

To qualify the SiNP-formulation *in vivo*, we immunized C57BL/6J mice in the following groups: PBS control group (group 1), stabilized S protein ectodomain (S-trimer) with monophosphoryl lipid A liposomes (MPLA) adjuvant (group 2), soluble RBD with MPLA (group 3), RBD-SiNP with MPLA (group 4), RBD-SiNP without adjuvant (group 5), and Tozinameran mRNA vaccine (group 6). The delivery route was subcutaneous for groups 1–5 and intramuscular for group 6. We chose these routes because nanoparticles have been shown to undergo enhanced transport in lymph nodes upon subcutaneous application and the main route currently used for mRNA vaccines is intramuscular. The groups comprised 5 mice for group 2–6 and 4 mice for the PBS control group. The immunization regimen (**Figure S5**) included three immunizations at day 0, day 14 and day 28. Mice were bled on day 14 (bleed 1), day 28 (bleed 2) and day 35 (bleed 3), each time point being 14 days after the previous immunization. The total amount of protein used per dose in groups 2–5 was 8 µg, as this amount induced high serum antibody levels in previous experiments [27]. Adjuvanted groups (groups 2–4) received 24 µg MPLA per immunization (corresponding to a 1:3 ratio (w/w) of immunogen to adjuvant) mixed with vaccine proteins in a total volume of 50 µl.

To ensure comparability with other studies, we included a group of mice receiving an mRNA vaccine. We chose a dose of 5 µg for the mRNA vaccine, as strong serum levels of S-binding antibodies have been reported for this dose [43].

3.8. S- and RBD-specific IgG responses

IgG responses at the final bleed (bleed 3) were quantified in an ELISA serum titration experiment where either the S-trimer or the RBD protein was coated to the ELISA plate. For both antigens, the highest antigen-specific antibody serum concentration was detected in the mice immunized with mRNA (**Figure 3A and B**).

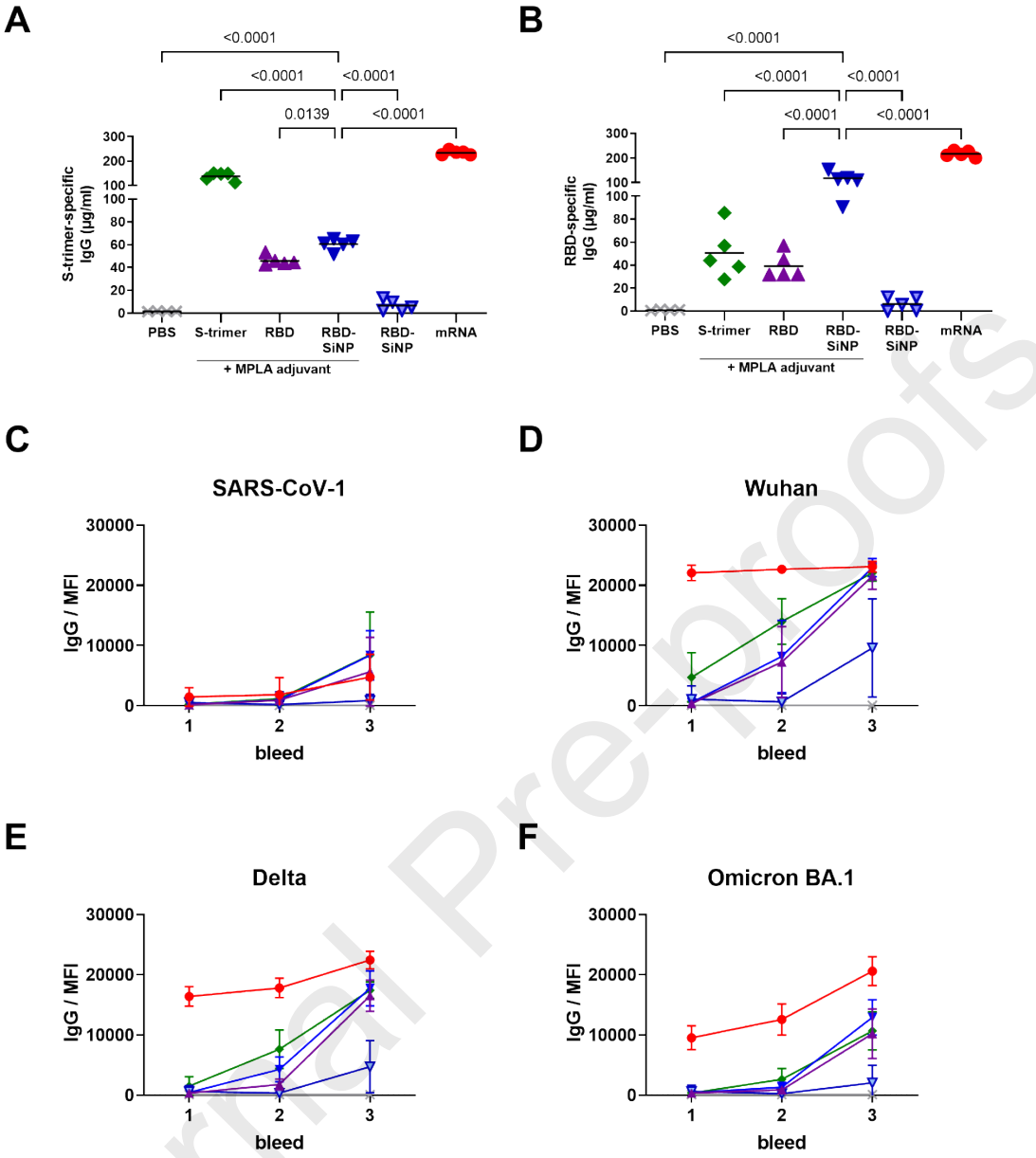

Figure 3: Antigen specific IgG serum concentrations and kinetics and breadth of IgG response. (A) S ectodomain-specific and (B) RBD-specific IgG response in µg/ml serum after three immunizations (bleed 3). The horizontal lines represent means. Statistical testing: Ordinary one-way ANOVA with Šídák's correction for multiple comparisons (for all comparisons with the adjuvanted RBD-SiNP vaccine p-values are given). (C-F) Serum reactivities at 1:500 serum dilution at the three bleeds against a panel of RBD variants in a Luminex multiplex assay. Reactivities against (C) SARS-CoV-1, (D) Wuhan-D614G, (E) VoC Delta, and (F) VoC Omicron sublineage BA.1.

The antibody response to the homologous immunogen used for immunization was found to be stronger than to the heterologous one. Furthermore, the addition of MPLA as adjuvant enhanced the immunogenicity of RBD-decorated SiNPs (RBD-SiNPs) with regards to antibody titers. Furthermore, in the presence of adjuvant, the response

against the RBD in the nanoparticulate delivery form was significantly stronger than in the soluble form measured against both antigens (S-trimer: p=0.0139; RBD: p<0.0001) and scored best except for the mRNA/LNP delivery, when the RBD instead of the complete S was used for the ELISA readout.

To further investigate the time course of induction of specific antibodies during the immunization experiment, we performed a Luminex multiplex antibody binding assay. For this purpose, four relevant variants of RBD variants (SARS-CoV-1, Wuhan-D614G, variant of concern [VoC] Delta, and VoC Omicron sublineage BA.1) were site-specifically biotinylated via a C-terminal avi-tag and loaded onto streptavidin-conjugated Luminex beads. The beads were multiplexed, incubated with a serum dilution of 1:500 (which optimally represents the dynamic range of the signal for all bleedings and antigens) and bound IgG was detected (**Figure 3C-F**). Similar to the serum concentrations determined for bleed 3, significantly higher serum antibody levels were observed after vaccination with the mRNA vaccine compared to the protein vaccines. It should be noted that exact replication of the antigen specific serum antibody concentrations determined in the ELISA format for bleed 3 could not be achieved due to the single dilution used in the Luminex assay. However, a differentiation of the induced serum reactivities among the protein-based vaccines was only recognizable for bleed 2 depending on the RBD variant used for the Luminex readout, respectively. In general, at the time of bleed 2, the reactivity of the sera immunized with S-trimer was slightly higher than that of the RBD sera. Also consistent with serum antibody concentrations, sera from animals vaccinated with non-adjuvanted RBD-SiNP showed generally reduced reactivity.

With regard to the breadth of reactivity of the antibodies towards the different VoC-RBDs tested here, the previously described reduced binding towards SARS-CoV-1, Delta and the Omicron variants in humans after infection and vaccination was recapitulated [30]. In this respect, we found no advantage of the nanoparticulate antigen delivery. Nanoparticulate delivery has been shown in the past to result in enhanced formation of germinal centers in secondary lymphoid organs [44]. As a consequence, an increased B cell maturation and thus enhanced antibody affinity maturation takes place, which can be investigated by serum avidity measurements. In previous work, we have found evidence of increased avidity in the SiNP-delivery of HIV-1 antigens in mice [27]. We tested the serum avidity against the four previously

used RBD variants in the sera of the adjuvanted RBD groups. Binding of the serum antibodies to the antigen was disrupted by 1 M NaSCN. The resulting avidity indices (AI) are shown in **Figure 4A.**

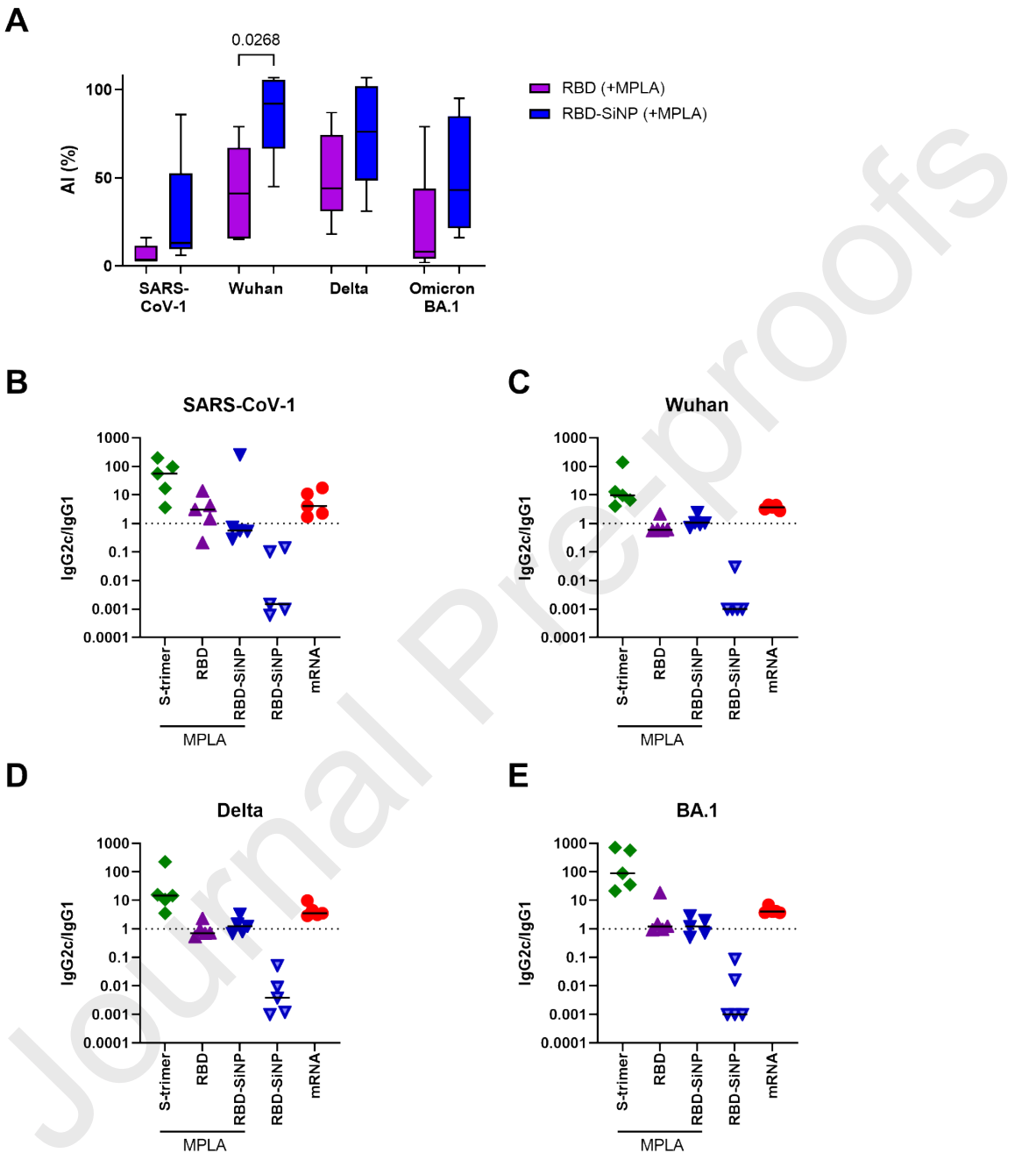

Figure 4: Serum avidity measurements and IgG_{2c}/IgG_1 ratio. Serum avidity was determined for mouse group 3 (RBD+MPLA) and mouse group 4 (RBD-SiNP +MPLA) against four different antigens (SARS-CoV-1, Wuhan, Delta, BA.1)**.** Serum avidity was measured by Luminex and avidity index (AI) values are given in percent (%). After binding of the serum antibodies, the Luminex beads were incubated with 1 M NaSCN or PBS. The AI is the ratio of detected signal of NaSCN/PBS-treated sample. Boxplot (1^{st} and 3^{rd} quartile) with whiskers (minimum to

maximum). Statistical testing: Friedman Test, with Dunn's correction for multiple comparisons (only the *p*-values with $p<0.05$ are shown). (B-E) IgG_{2c}/IgG_1 ratio: reactivities were determined by Luminex using anti-mouse subtype specific secondary antibodies. The dashed line indicates a ratio of 1. Horizontal lines represent medians. Ratios were determined for relevant antigens: (B) SARS-CoV-1, (C) SARS-CoV-2 Wuhan D614G, (D) SARS-CoV-2 Delta, (E) SARS-CoV-2 Omicron sublineage BA.1.

Higher AI values in the SiNP-group as compared to the soluble RBD group were found for all tested antigens, reaching significance in case of the homologous RBD-Wuhan immunogen. Consequently, for the RBD-SiNP group a more pronounced affinity maturation of Wuhan strain-specific B cells can be deduced.

The B-cell response is coordinated by a tightly regulated T-cell response [45]. In order to gain insight regarding the impact of our RBD formulations on T helper (T_h) cell polarization we determined the IgG_{2c}/IgG_1 ratio. IgG_{2c}/IgG_1 ratios of ≥ 1 is generally considered to correspond to a strong T_h1 response, and has been associated with protective immune response e.g. in *Leishmania tropica* infection [46], whereas ratios of <1 are rather indicative for a T_h2 type response, which is commonly associated with allergic reactions. Furthermore, T_h1 responses are related to a strong cellular immune response (e.g. CD8 T cell responses) and T_h2 responses are related to a strong humoral immune response (e.g. B cell response). Consequently, we determined the reactivities of the four IgG subtypes in the sera of our immunization study using the previously described Luminex method (**Figure S6**). The resulting IgG_{2c}/IgG_1 ratios are shown in **Figure 4B-E**.

Of all five antigens tested, sera from mice immunized with S-trimer displayed the highest median IgG_{2c}/IgG_1 ratio followed by the mRNA vaccine sera. As expected, formulation with MPLA adjuvant generally drove the immune response towards a T_h1 response for all constructs. While S-trimer with MPLA resulted in a strong T_h1 response, the response was more balanced in case of the MPLA-adjuvanted RBD. The presentation via SiNP had no influence on the T_h response, as can be deduced from the comparison of group 3 (soluble RBD with MPLA) and group 4 (RBD-SiNP with MPLA).

3.9. T cell response

To directly investigate the vaccine induced amounts of antigen specific $CD4^+$ and $CD8^+$ T cells, we performed intracellular staining for selected cytokines (interferon-γ [IFNγ], interleukin-2 [IL-2], and tumor-necrosis factor alpha [TNFα]) and determined the

amount of secreted cytokines (IFNγ, interleukin-4 [IL-4], and interleukin-5 [IL-5]) produced by T cells upon antigen-specific stimulation. IFNγ, IL-2, TNFα are central cytokines expressed at different stages of central effector and memory T-cell differentiation (T_{CE} and T_{CM} cells). Naïve $CD4^+$ or $CD8^+$ T cells differentiate into multifunctional T cells with a cytokine profile optimized for their effector function (such as IFNγ, IL-2, TNFα) along their differentiation towards T_{CM} cells [47]. The secreted cytokine profile can inform on the T helper cell polarization of the T cell response: IFNγ is the central T_h1 cytokine, whereas IL-4 and IL-5 are typically secreted during T_h2 polarization.

We first used two spike-specific peptide pools for stimulation of the $CD4^+$ or $CD8^+$ T cells (isolated from the spleens at the endpoint of analysis), representing the S1 and the S2 domain of the SARS-CoV-2 spike protein, respectively. Since the RBD is part of the S1 domain, the groups immunized with RBD constructs could only respond to stimulation with the S1 pool. After stimulation and subsequent intracellular staining, the cells were analyzed by flow cytometry (**Figure 5**).

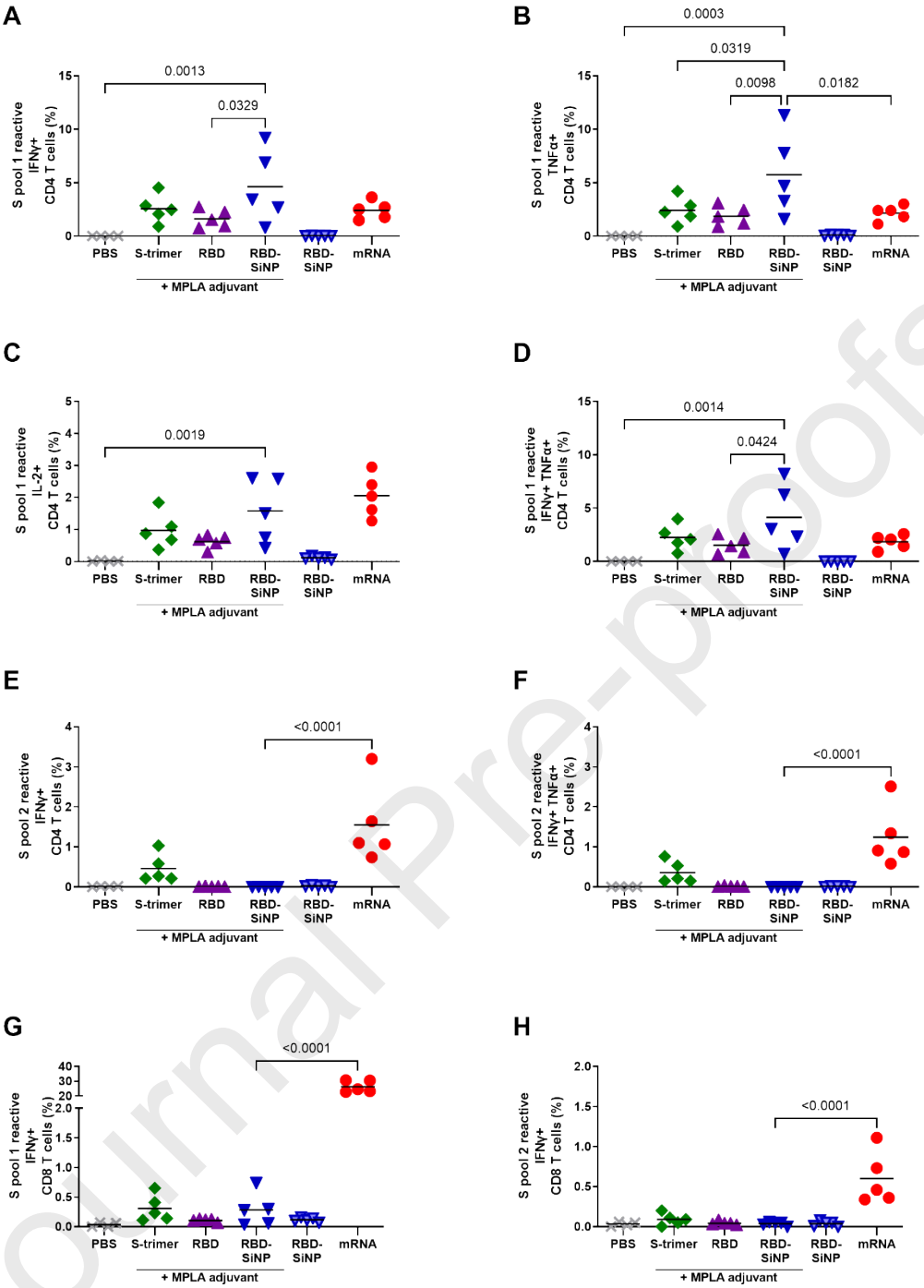

Figure 5: CD4⁺ and CD8⁺ T cell responses upon stimulation with spike-specific peptide pools S pool 1 and S pool 2. Responses were measured in splenocytes at the final bleed (bleed 3). Cell numbers were quantified in percent of the total CD4⁺ or CD8⁺ cell population within the sample by flow cytometry. CD4⁺ cells were stained by intracellular staining against (A) IFNγ, (B) TNFα, (C) IL-2, and (D) IFNγ+TNFα after stimulation with S pool 1. (E) IFNγ and (F) IFNγ/TNFα double positive cells after stimulation with S pool 2. (G) S pool 1 reactive and (H) S pool 2 reactive IFNγ CD8⁺ T cells. The horizontal lines represent means. Statistical testing: Ordinary one-way ANOVA with Šídák's correction for multiple comparisons (*p*-values are given). Note: only the *p*-values with $p<0.05$ from comparisons with group 4 are shown.

MPLA adjuvanted RBD-SiNPs induced the highest median levels of IFNγ, TNFα, and IFNγ/TNFα double positive multifunctional $CD4^+$ T cell counts. For IL-2 MPLA adjuvanted RBD-SiNPs showed the highest $CD4^+$ T cell responses among the protein-based vaccines (group 2-5). As expected, the number of S pool 1 and S-pool 2 reactive $CD8^+$ T cells was markedly increased in mRNA-vaccinated animals as compared to animals vaccinated with protein-based vaccines. In summary, immunization with adjuvanted RBD-SiNP elicited strong and multifunctional S pool 1-specific $CD4^+$ T-cell responses whilst the numbers of $CD8^+$ IFNγ producing cells corresponding to T_{CM}, or terminal effector T cells were low.

Besides the quantity of T cell subsets, the levels of selected cytokines produced is also of interest, in order to analyze a potential underlying T_h1- or T_h2-polarization as well as the activation status of the respective cells. To determine the amount of IFNγ, IL-4 and IL-5 defined numbers of splenocytes were stimulated with spike protein and the cytokines produced in the supernatant were quantified (**Figure 6**).

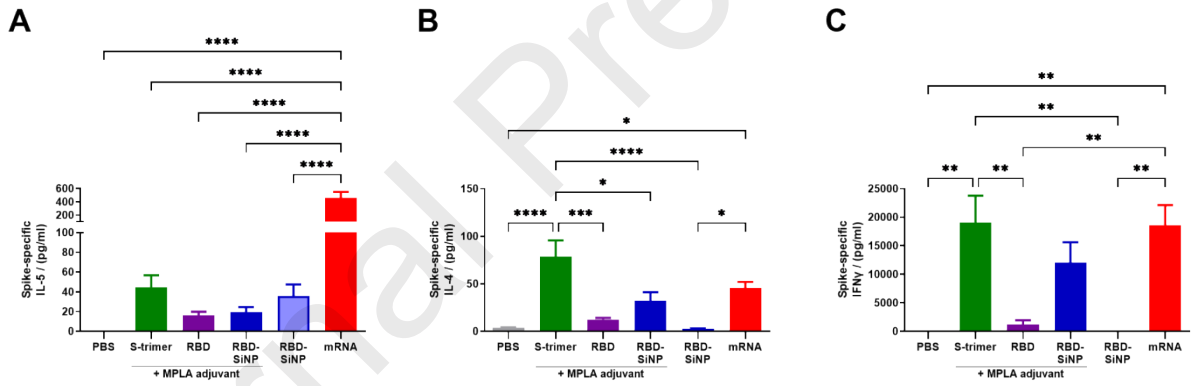

Figure 6: S-specific cytokine production in splenocytes. Splenocytes were stimulated with 2 µg/ml of SARS-CoV-2 S ectodomain protein for 48-hour at 37 °C, and the supernatants analyzed for secreted IFNγ, IL-4 and IL-5 by ELISA. Mean with standard error is displayed. Statistical testing: Ordinary one-way ANOVA with Šídák's correction for multiple comparisons (*p*-values with $p<0.05$ are given).

A significantly stronger IL-5 secretion was apparent upon stimulation for the mRNA group. Secretion levels of IL-4 and IFNγ were comparable between the S-trimer-, RBD-SiNP- (both adjuvanted with MPLA), and the mRNA-group.

3.10. Pseudotype Neutralization

To determine breadth and potency of the neutralization capacity of the sera, we performed lentiviral pseudotype neutralization assays (**Figure 7**). The lentiviral

particles were pseudotyped with the S proteins of the SARS-CoV-2 variant Wuhan D614G, and of the VoCs Delta and Omicron BA.1. To enable efficient infection, the host cells transiently express human ACE2.

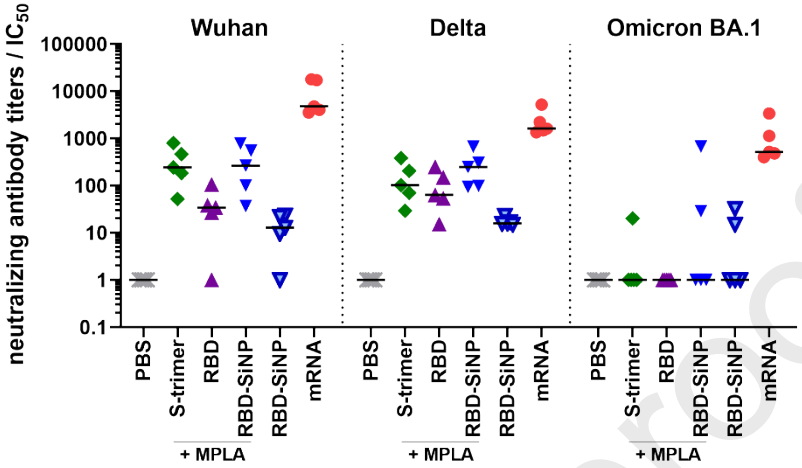

Figure 7: Determination of the neutralization capacity of the sere by pseudotype neutralization. Pseudotype virus variants used expressed the S proteins of the SARS-CoV-2 variant Wuhan D614G, and of the VoC Delta and Omicron BA.1. IC_{50} values of titration experiments (n=3) are given. The horizontal lines represent medians.

The neutralization titers determined for the protein vaccines were by a factor 10 lower than the titers determined for the mRNA vaccine for all tested pseudotypes. In general, the neutralization titers largely reflect the S-specific IgG response – in fact, the neutralization titers appeared to represent a mixture of S- and RBD-specific binding titers (compare **Figure 4A and B**). Remarkably, the median Wuhan- and Delta-specific neutralization titer of the adjuvanted RBD-SiNP group is similar to that of the S-trimer group and – by trend – superior as compared to the adjuvanted RBD group. Other than the mRNA group, most animals immunized with the different protein vaccines did with few exceptions not develop Omicron specific neutralizing antibodies.

3.11. Ratio of serum neutralization titers to RBD-binding IgG

By normalizing the Wuhan strain specific pseudotype neutralization by the amounts of binding antibodies, the quality of the induced antibodies can be estimated (**Figure S7**). Highest ratios were found for the mRNA group followed by the S-trimer protein. The ratios for the RBD-groups were higher for the nanoparticle groups as compared to the soluble protein indicating a higher quality in terms of neutralization capacity for the individual antibodies induced.

4. Discussion

In the present work, our aim was to investigate the possibility of compensating for the low immunogenicity of the RBD of SARS-CoV-2's S protein by its oriented display on the surface of 100 nm solid SiNPs. The multivalent display of RBD has been shown to overcome the limited immunogenicity of the monomeric antigen in mice and macaques [48–50]. Furthermore, several studies reported that dimeric or trimeric multimerization of the RBD can improve immunogenicity [51–54]. Lastly, to date, seven clinical trials have investigated RBD as a vaccine antigen – three of them with multimerized RBDs (ZF2001, tandem-repeat dimeric RBD, [55]; FINLAY-FR-2, six RBDs coupled to one tetanus toxoid molecule, [56]; GBP510, self-assembling two-component nanoparticle displaying the RBD, [57]).

We decided to use a biorthogonal covalent coupling strategy to immobilize the RBD to the surface of the nanoparticles. To this end, we utilized a tandem-cysteine tag in combination with maleimide-chemistry, which have proven efficient when coupling HIV Env trimers to SiNPs recently [27,28]. In line with previous findings, attachment of the NtCC-tag to the N-terminus of the RBD and mild reduction by TCEP had no effect on the structural properties of the protein, as found in biophysical analyses and ELISA experiments with the structure-dependent antibodies S309, CR3022 as well as soluble ACE2.

The intrinsic stability of the nanoparticulate vaccine delivery platform is considered a key factor in reaching the lymph nodes before particle degradation and achieving an optimal immune response [13,26,58]. Hence, we chose solid SiNPs as delivery platform for its stability under storage and physiological conditions, for its versatile surface properties for further modifications, for its narrow size distribution and also because of its low toxicity *in vivo* [59,60]. We chose SiNPs with a size of 100 nm, since a size between 20 and 200 nm is considered optimal for passive transport in the lymphatic system and into the lymph nodes, while smaller or larger particles are mainly transported via APCs [13,60–66]. The coupling of the antigen was achieved by Michael addition to cysteines (protein) and primary amines (nanoparticle) using the heterobifunctional crosslinker sulfo-SMCC. The feasibility of coupling antigens with high molecular weights from 66 kDa to 215 kDa to the surface of SiNPs in a targeted and site-specific manner has been well-established [26–28,67,68]. In order to determine the reaction conditions that require the lowest possible protein amounts,

lead to homogeneous particle preparations and realize an optimal antigen density for interaction with B cells with a center-to-center distance 10–15 nm [42], coupling was performed at different ratios of available NH_2-groups on the SiNP surface to applied RBD. Similar to previous results, a ratio of 1:3 to 1:6 in combination with a 2-step wash-protocol proved to be optimal [26–28].

As expected, we measured an increase in the size of the particles after conjugation, which is due to the addition of the linker and the protein. Furthermore, we found that higher ratios of protein to NH_2-groups led to a further increased hydrodynamic diameter. It is likely that the higher amount of non-covalently bound protein on the SiNP surface is the cause of the additional increase in size. However, with a hydrodynamic diameter between 120 and 125 nm, the conjugates fit within the size range of the optimized lymph node targeting. Furthermore, we determined a PDI below 0.1 for our conjugates, which indicates a monodisperse particle preparation [61,66].

Next, we investigated the stability of the protein-conjugated particle preparations. The stability of the attachment of the RBD to the SiNP surface under straightforward storage conditions (4 °C) as well as under *in vivo* conditions (37 °C) is of crucial importance for both practical usability and efficacy. We found minimal release of coupled protein from the particles over an extended period of 120 days at both temperatures. The occurring RBD release from the SiNP surface is likely caused by the retro-Michael reaction [69]. Colloidal stability is another important stability parameter of a nanoparticle vaccine, as agglomeration would alter functionality of the vaccine by changing the route of trafficking to the lymph node and loss of activity due to changes in the effective local concentration of the antigen. We found no marked changes of the RBD-SiNP size at 4 °C or 37 °C. While almost no change in the PDI was observed at 4 °C, a slight increase up to 0.09 was observed at 37 °C.

By characterizing the particles with antibodies or ligands binding to different parts of the antigen, the structural integrity as well as the orientation and thus the accessibility of the antigen for B cell receptors directed to the respective epitopes can be studied. We tested the antigenicity of the RBD-SiNP conjugates in an MST binding study. MST has been shown to be suitable for nanoparticle-antigen-antibody binding analysis [65]. Furthermore, we analyzed the functionality of the RBM with an ACE2 activity competition assay. The RBM is the central epitope in eliciting competitive neutralizing

antibodies and binding to ACE2 proves its structural integrity. We found the antibodies S309 and CR3022 and soluble ACE2 to bind to RBD after coupling with K_d values in the nanomolar range. In an ACE2 inhibition assay, for the soluble RBD only up to 29% ACE2 activity reduction was detectable, while with the nanoparticle-bound RBD a concentration dependent ACE2 activity reduction up to 70% was achieved. The results of the MST antibody binding studies showed the different accessibility of the epitopes depending on their localization and therefore proved the oriented coupling of the antigen. The concentration-dependent reduction of the ACE2 activity by RBD-SiNP further proved and the structural integrity of the RBM and thus the functionality of the coupled RBD.

APCs play a crucial role in the effective immune response by presenting antigen to immune cells, by activating reactive T cells, and by transporting antigen to the secondary lymphoid organs [70]. Physicochemical properties of nanoparticles such as size, surface chemistry and shape influence their uptake efficiency [71]. In addition, the structure and post-translational modifications of the antigen have been shown to influence the uptake properties [44]. We examined the *in vitro* interaction with APCs by evaluating the internalization of the RBD-SiNPs into mouse BMDCs. We did not observe enhanced uptake of RBD-SiNPs compared to soluble RBDs. Apparently, conjugation to SiNP does not provide an advantage in uptake over soluble RBD in our experimental setup. Nevertheless, the antigen structure-preserving transport of the nanoparticles on the cell surface of the DCs into the lymph nodes could represent an advantage that was not detectable in our simplified *in vitro* test. Biodistribution of antigen-loaded SiNPs, their uptake into lymph nodes and their potential for efficient induction of germinal center formation are interesting further questions to be investigated in future experiments.

To qualify the immunogenicity of the RBD-SiNP-vaccine *in vivo*, we performed a mouse immunization study. To allow for comparisons with earlier mouse immunization studies and the BMDC uptake experiments, we immunized C57BL/6J mice. Similar to earlier experiments, the MPLA (non-toxic lipopolysaccharide) was used as an adjuvant [27]. MPLA displays the immune-stimulatory properties of LPS, a potent TLR4-agonist [72,73]. We compared our adjuvanted RBD-SiNP-vaccine with adjuvanted soluble RBD, adjuvanted S ectodomain trimer, and non-adjuvanted RBD-SiNP-vaccine.

Furthermore, we included BioNTech/Pfizer's state-of-the art mRNA vaccine BNT162b2 (Tozinameran), as a benchmark.

When analyzing the induced antigen-specific antibody levels we found significantly higher RBD-specific IgG serum concentrations for the MPLA-adjuvanted RBD-SiNP as compared to the adjuvanted soluble RBD and S protein at the terminal bleed (both $p<0.0001$). The RBD-specific serum IgG levels induced by the adjuvanted RBD-SiNP reached 54% of the levels induced by the mRNA vaccine, as judged by the medians. The markedly lower IgG levels induced by the non-adjuvanted RBD-SiNPs demonstrate the need for co-stimulation of the innate and adaptive immune responses by an adjuvant. In this context, optimizing the type, formulation and dosage of the adjuvant used in combination with the nanoparticulate antigen is a relevant subject of current research. We could not observe any difference in induced titers of the nanoparticle vaccines over time and with respect to breadth of binding as compared to the other adjuvanted protein formulations.

On the cellular arm of immunity, the MPLA adjuvanted RBD-SiNPs elicited strong and multifunctional spike-specific $CD4^+$ T cell responses. Polyfunctional $CD4^+$ T cells provide a more effective immune response than other functional subsets that produce only a single cytokine [74]. Of note, polyfunctional $CD4^+$ T have been shown for example to correlate with a reduced risk of infection in the RV144 HIV-1 prophylactic HIV vaccination trial ("Thai Trial") [75]. Contrary to the $CD4^+$ response, the levels of antigen specific $CD8^+$ T_{CM},T_{EM}, or terminal effector cells were low in all protein-groups. In accordance with recent reports from the human COVID-19 vaccination campaigns, high levels of $CD8^+$ T cells were induced by the SARS-CoV-2 mRNA vaccine [76]. Although $CD8^+$ T cells have been discussed as the main mediator of protection in the early post-vaccination phase [77], $CD8^+$ T cell exhaustion has been described in cases of COVID-19, associated with progressive impairment of effector functions [78]. It is currently unclear which role $CD8^+$ T cells play, particularly in long-term immunity after vaccination. When analyzing the T_h polarization, both T_h2 cytokine IL-4 and T_h1 cytokine IFNγ were profoundly secreted after the immunization of the S-trimer-, RBD-SiNP-, and the mRNA-groups, which suggests balanced T_h polarization for these groups and may indicate an induction of T_{FH} cells as inferred from the detected IL-4 levels [79]. Apart from the secretion of IL-4 and IFNγ, a significantly stronger T_h2

cytokine IL-5 upon stimulation for the mRNA group in comparison to all other groups was found.

We determined pseudotype neutralization as a functional measure of immunity and a well-defined correlate of protection against infection with SARS-CoV-2 [80,81]. In accordance with the serum concentrations induced by the different vaccines, highest neutralizing titers were found for the mRNA vaccine. For adjuvanted proteins, S-trimer-induced titers exceeded soluble RBD-induced titers by a factor of 7.1, as judged by the medians. Interestingly, in the case of the Wuhan pseudotype, SiNP administration was able to match the neutralization to the level of the S-trimer. In the case of Delta, this could even be exceeded by SiNP administration (factor 2.4, comparison of medians, no significance). Neutralization of the Omicron variant, which contains many mutations mainly in the RBD, could only be shown for the mRNA group (with the exception of individual mice from SiNP- and S-trimer groups).

As a measure for the quality of the induced neutralizing antibody response, we analyzed the ratios of the Wuhan pseudotype neutralization and serum concentration of autologous antigen-reactive IgG. The quality can be regarded as a combination of the number of neutralizing epitopes targeted and the avidity and affinity of the corresponding antibodies. We found lower ratios for the RBD as compared to the S-trimer. Interestingly such difference was also reported for the same ratio induced by the mRNA vaccine BNT162b1 (encoding the RBD) in comparison to the ratio determined in convalescent plasma [82]. This difference was partially explained by enhanced induction of neutralizing epitopes outside the RBD by the S ectodomain on the virion. In our experiment, SiNP-based delivery of RBD apparently compensated for this. Whether this indicates enhanced activity within the germinal centers and thus enhanced affinity maturation, as shown in other cases for nanoparticulate delivery, remains to be investigated [44].

5. Conclusion

In the presented work, we found additional evidence for the suitability of non-porous silica nanoparticles as adaptable and stable vaccine delivery platform. We successfully immobilized the SARS-CoV-2 RBD in a site-specific and stable manner. This directed orientation of the antigen on the surface of the particles maintains the accessibility of different antibody epitopes and allows for ACE2 binding. With the nanoparticle-RBD conjugate, we achieved recognition and internalization by BMDCs *in vitro*. In a mouse immunization study, MPLA adjuvanted RBD-SiNPs induced high S- and RBD-specific IgG serum concentrations, strong S pool 1-specific $CD4^+$ T-cell responses and weak S pool 1-specific $CD8^+$ T-cell responses, and a balanced T helper response. By SiNPs-delivery, the induced neutralization could be improved compared to the soluble RBD. RBD-SiNP titers reached homologous and exceeded heterologous (Delta) neutralization capacity induced by the soluble S-trimer. Serum avidity and the ratio of neutralization titers to serum antibody concentrations indicated an increased affinity maturation induced by the adjuvanted RBD-SiNP vaccine. Thus, the SiNP-based vaccine delivery system is promising for further preclinical and clinical investigations.

6. Acknowledgement

The authors want to acknowledge the team from 2bind (Regensburg, Germany) for the opportunity to use their MST devices and the excellent technical assistance by Merve Gökalp and Renate Liebl (University Regensburg). We thank Theresa Asen, and Susanne Miko (Technical University Munich) for their excellent technical support during the mouse studies. We also thank Lisa Zeller, Jonas Holzinger and Prof. Dr. Dr. André Gessner (Institute of Medical Microbiology and Hygiene, University Regensburg) for providing mouse BMDCs and Prof. Dr. Stefan Pöhlmann (Georg-August-University Göttingen) for providing HEK-293T-ACE2 cells.

7. Funding

This work received funding from the States Ministry of Science and Art, Bavaria, Germany (Grant ForCOVID to UP, RW and DP) and by the German Ministry of Health and Education (BMBF, Rahmenprogramm Gesundheitsforschung "Wirkstofftransport"; Project HIVacToGC (coordination RW), grant agreement No. 16GW0393K).

8. Author contributions (CRediT author statement)

Conceptualization, D.P., M.Br., and R.W.; formal analysis, D.P., C.B. and J.S.; methodology, D.P., C.B., J.S. M.Bi., G.C.; investigation C.B., J.S., N.S., R.B., M.Bi., and D.P.; data curation, D.P., C.B., and, J.S.; writing – original draft preparation, D.P. and C.B.; writing – review and editing, D.P., C.B., J.S., M.Br., and R.W.; visualization, D.P. and C.B.; project administration, D.P. M.Br., J.H., N.T., U.P., and R.W.; supervision, D.P., M.Br., J.H., U.P., and R.W.; funding acquisition, D.P., R.W., U.P. and M.Br.. All authors have read and agreed to the published version of the manuscript.

9. Disclosure

All authors declare no competing interests regarding this study content. Given their role as Guest Editors, Miriam Breunig and Ralf Wagner had no involvement in the peer-review of this article and had no access to information regarding its peer-review.

10. References

1. Lee WS, Wheatley AK, Kent SJ, DeKosky BJ. Antibody-dependent enhancement and SARS-CoV-2 vaccines and therapies. Nat Microbiol. 2020;5:1185–91.

2. Walsh EE, Frenck RW, Falsey AR, Kitchin N, Absalon J, Gurtman A, et al. Safety and Immunogenicity of Two RNA-Based Covid-19 Vaccine Candidates. N Engl J Med. 2020;383:2439–50.

3. Dai L, Gao GF. Viral targets for vaccines against COVID-19. Nat Rev Immunol. 2021;21:73–82.

4. Mandolesi M, Sheward DJ, Hanke L, Ma J, Pushparaj P, Perez Vidakovics L, et al. SARS-CoV-2 protein subunit vaccination of mice and rhesus macaques elicits potent and durable neutralizing antibody responses. Cell Reports Medicine. 2021;2:100252.

5. Zhang B-Z, Wang X, Yuan S, Li W, Dou Y, Poon VK-M, et al. A novel linker-immunodominant site (LIS) vaccine targeting the SARS-CoV-2 spike protein protects against severe COVID-19 in Syrian hamsters. Emerging Microbes & Infections. 2021;10:874–84.

6. Hattori T, Koide A, Noval MG, Panchenko T, Romero LA, Teng KW, et al. The ACE2-binding Interface of SARS-CoV-2 Spike Inherently Deflects Immune Recognition. Journal of Molecular Biology. 2021;433:166748.

7. Heidary M, Kaviar VH, Shirani M, Ghanavati R, Motahar M, Sholeh M, et al. A Comprehensive Review of the Protein Subunit Vaccines Against COVID-19. Front Microbiol. 2022;13:927306.

8. Jennings GT, Bachmann MF. The coming of age of virus-like particle vaccines. Biol Chem. 2008;389:521–36.

9. Ludwig C, Wagner R. Virus-like particles—universal molecular toolboxes. Current Opinion in Biotechnology. 2007;18:537–45.

10. Asbach B, Wagner R. Particle-based delivery of the HIV envelope protein. Current Opinion in HIV and AIDS. 2017;12:265–71.

11. Chattopadhyay S, Chen J-Y, Chen H-W, Hu C-MJ. Nanoparticle Vaccines Adopting Virus-like Features for Enhanced Immune Potentiation. Nanotheranostics. 2017;1:244–60.

12. Irvine DJ, Swartz MA, Szeto GL. Engineering synthetic vaccines using cues from natural immunity. Nature Mater. 2013;12:978–90.

13. Thalhauser S, Peterhoff D, Wagner R, Breunig M. Critical design criteria for engineering a nanoparticulate HIV-1 vaccine. Journal of Controlled Release. 2020;317:322–35.

14. Nguyen B, Tolia NH. Protein-based antigen presentation platforms for nanoparticle vaccines. npj Vaccines. 2021;6:70.

15. Zhao L, Seth A, Wibowo N, Zhao C-X, Mitter N, Yu C, et al. Nanoparticle vaccines. Vaccine. 2014;32:327–37.

16. Swartz MA, Hirosue S, Hubbell JA. Engineering Approaches to Immunotherapy. Sci Transl Med [Internet]. 2012 [cited 2023 May 17];4. Available from: https://www.science.org/doi/10.1126/scitranslmed.3003763

17. Rudra JS, Tian YF, Jung JP, Collier JH. A self-assembling peptide acting as an immune adjuvant. Proc Natl Acad Sci U S A. 2010;107:622–7.

18. Shirai S, Kawai A, Shibuya M, Munakata L, Omata D, Suzuki R, et al. Lipid Nanoparticle Acts as a Potential Adjuvant for Influenza Split Vaccine without Inducing Inflammatory Responses. Vaccines. 2020;8:433.

19. Brinkkemper M, Sliepen K. Nanoparticle Vaccines for Inducing HIV-1 Neutralizing Antibodies. Vaccines (Basel). 2019;7:76.

20. Marcandalli J, Fiala B, Ols S, Perotti M, De Van Der Schueren W, Snijder J, et al. Induction of Potent Neutralizing Antibody Responses by a Designed Protein Nanoparticle Vaccine for Respiratory Syncytial Virus. Cell. 2019;176:1420-1431.e17.

21. Boyoglu-Barnum S, Ellis D, Gillespie RA, Hutchinson GB, Park Y-J, Moin SM, et al. Quadrivalent influenza nanoparticle vaccines induce broad protection. Nature. 2021;592:623–8.

22. Bruun TUJ, Andersson A-MC, Draper SJ, Howarth M. Engineering a Rugged Nanoscaffold To Enhance Plug-and-Display Vaccination. ACS Nano. 2018;12:8855–66.

23. Zhao Q, Li S, Yu H, Xia N, Modis Y. Virus-like particle-based human vaccines: quality assessment based on structural and functional properties. Trends in Biotechnology. 2013;31:654–63.

24. Metz SW, Tian S, Hoekstra G, Yi X, Stone M, Horvath K, et al. Precisely Molded Nanoparticle Displaying DENV-E Proteins Induces Robust Serotype-Specific Neutralizing Antibody Responses. Beasley DWC, editor. PLoS Negl Trop Dis. 2016;10:e0005071.

25. Mody KT, Popat A, Mahony D, Cavallaro AS, Yu C, Mitter N. Mesoporous silica nanoparticles as antigen carriers and adjuvants for vaccine delivery. Nanoscale. 2013;5:5167.

26. Thalhauser S, Peterhoff D, Wagner R, Breunig M. Presentation of HIV-1 Envelope Trimers on the Surface of Silica Nanoparticles. Journal of Pharmaceutical Sciences. 2020;109:911–21.

27. Peterhoff D, Thalhauser S, Sobczak JM, Mohsen MO, Voigt C, Seifert N, et al. Augmenting the Immune Response against a Stabilized HIV-1 Clade C Envelope Trimer by Silica Nanoparticle Delivery. Vaccines. 2021;9:642.

28. Peterhoff D, Thalhauser S, Neckermann P, Barbey C, Straub K, Nazet J, et al. Multivalent display of engineered HIV-1 envelope trimers on silica nanoparticles for targeting and in vitro activation of germline VRC01 B cells. Eur J Pharm Biopharm. 2022;181:88–101.

29. Peterhoff D, Glück V, Vogel M, Schuster P, Schütz A, Neubert P, et al. A highly specific and sensitive serological assay detects SARS-CoV-2 antibody levels in COVID-19 patients that correlate with neutralization. Infection. 2021;49:75–82.

30. Mader A-L, Tydykov L, Glück V, Bertok M, Weidlich T, Gottwald C, et al. Omicron's binding to sotrovimab, casirivimab, imdevimab, CR3022, and sera from previously infected or vaccinated individuals. iScience. 2022;25:104076.

31. Schatz PJ. Use of Peptide Libraries to Map the Substrate Specificity of a Peptide-Modifying Enzyme: A 13 Residue Consensus Peptide Specifies Biotinylation in Escherichia coli. Nat Biotechnol. 1993;11:1138–43.

32. Lutz MB, Kukutsch N, Ogilvie ALJ, Rößner S, Koch F, Romani N, et al. An advanced culture method for generating large quantities of highly pure dendritic cells from mouse bone marrow. Journal of Immunological Methods. 1999;223:77–92.

33. Moeini H, Afridi SQ, Donakonda S, Knolle PA, Protzer U, Hoffmann D. Linear B-Cell Epitopes in Human Norovirus GII.4 Capsid Protein Elicit Blockade Antibodies. Vaccines. 2021;9:52.

34. Hauser A, Carnell G, Held K, Sulbaran G, Tischbierek N, Rogers L, et al. Stepwise Conformational Stabilization of a HIV-1 Clade C Consensus Envelope Trimer Immunogen Impacts the Profile of Vaccine-Induced Antibody Responses. Vaccines. 2021;9:750.

35. Festag MM, Festag J, Fräßle SP, Asen T, Sacherl J, Schreiber S, et al. Evaluation of a Fully Human, Hepatitis B Virus-Specific Chimeric Antigen Receptor in an Immunocompetent Mouse Model. Molecular Therapy. 2019;27:947–59.

36. Kosinska AD, Moeed A, Kallin N, Festag J, Su J, Steiger K, et al. Synergy of therapeutic heterologous prime-boost hepatitis B vaccination with CpG-application to improve immune control of persistent HBV infection. Sci Rep. 2019;9:10808.

37. Hoffmann M, Arora P, Groß R, Seidel A, Hörnich BF, Hahn AS, et al. SARS-CoV-2 variants B.1.351 and P.1 escape from neutralizing antibodies. Cell. 2021;184:2384-2393.e12.

38. Naldini L, Blömer U, Gallay P, Ory D, Mulligan R, Gage FH, et al. In Vivo Gene Delivery and Stable Transduction of Nondividing Cells by a Lentiviral Vector. Science. 1996;272:263–7.

39. Zufferey R, Nagy D, Mandel RJ, Naldini L, Trono D. Multiply attenuated lentiviral vector achieves efficient gene delivery in vivo. Nat Biotechnol. 1997;15:871–5.

40. Carnell G, Grehan K, Ferrara F, Molesti E, Temperton N. An Optimized Method for the Production Using PEI, Titration and Neutralization of SARS-CoV Spike Luciferase Pseudotypes. BIO-PROTOCOL [Internet]. 2017 [cited 2023 May 17];7. Available from: https://bio-protocol.org/e2514

41. Genova C, Sampson A, Scott S, Cantoni D, Neto M, Bentley E, et al. Production, Titration, Neutralisation, Storage and Lyophilisation of Severe Acute Respiratory Syndrome Coronavirus 2 (SARS-CoV-2) Lentiviral Pseudotypes. BIO-PROTOCOL [Internet]. 2021 [cited 2023 May 17];11. Available from: https://bio-protocol.org/e4236

42. Tokatlian T, Kulp DW, Mutafyan AA, Jones CA, Menis S, Georgeson E, et al. Enhancing Humoral Responses Against HIV Envelope Trimers via Nanoparticle Delivery with Stabilized Synthetic Liposomes. Sci Rep. 2018;8:16527.

43. Vogel AB, Kanevsky I, Che Y, Swanson KA, Muik A, Vormehr M, et al. BNT162b vaccines protect rhesus macaques from SARS-CoV-2. Nature. 2021;592:283–9.

44. Tokatlian T, Read BJ, Jones CA, Kulp DW, Menis S, Chang JYH, et al. Innate immune recognition of glycans targets HIV nanoparticle immunogens to germinal centers. Science. 2019;363:649–54.

45. Cyster JG, Allen CDC. B Cell Responses: Cell Interaction Dynamics and Decisions. Cell. 2019;177:524–40.

46. Rostamian M, Sohrabi S, Kavosifard H, Niknam HM. Lower levels of IgG1 in comparison with IgG2a are associated with protective immunity against Leishmania tropica infection in BALB/c mice. Journal of Microbiology, Immunology and Infection. 2017;50:160–6.

47. Seder RA, Darrah PA, Roederer M. T-cell quality in memory and protection: implications for vaccine design. Nat Rev Immunol. 2008;8:247–58.

48. Wang Y, Wang L, Cao H, Liu C. SARS-CoV-2 S1 is superior to the RBD as a COVID-19 subunit vaccine antigen. J Med Virol. 2021;93:892–8.

49. Walls AC, Fiala B, Schäfer A, Wrenn S, Pham MN, Murphy M, et al. Elicitation of Potent Neutralizing Antibody Responses by Designed Protein Nanoparticle Vaccines for SARS-CoV-2. Cell. 2020;183:1367-1382.e17.

50. Dalvie NC, Tostanoski LH, Rodriguez-Aponte SA, Kaur K, Bajoria S, Kumru OS, et al. SARS-CoV-2 receptor binding domain displayed on HBsAg virus–like particles elicits protective immunity in macaques. Sci Adv. 2022;8:eabl6015.

51. An Y, Li S, Jin X, Han J, Xu K, Xu S, et al. A tandem-repeat dimeric RBD protein-based covid-19 vaccine zf2001 protects mice and nonhuman primates. Emerging Microbes & Infections. 2022;11:1058–71.

52. Pan X, Shi J, Hu X, Wu Y, Zeng L, Yao Y, et al. RBD-homodimer, a COVID-19 subunit vaccine candidate, elicits immunogenicity and protection in rodents and nonhuman primates. Cell Discov. 2021;7:82.

53. Routhu NK, Cheedarla N, Bollimpelli VS, Gangadhara S, Edara VV, Lai L, et al. SARS-CoV-2 RBD trimer protein adjuvanted with Alum-3M-052 protects from SARS-CoV-2 infection and immune pathology in the lung. Nat Commun. 2021;12:3587.

54. Sun W, He L, Zhang H, Tian X, Bai Z, Sun L, et al. The self-assembled nanoparticle-based trimeric RBD mRNA vaccine elicits robust and durable protective immunity against SARS-CoV-2 in mice. Sig Transduct Target Ther. 2021;6:340.

55. Dai L, Zheng T, Xu K, Han Y, Xu L, Huang E, et al. A Universal Design of Betacoronavirus Vaccines against COVID-19, MERS, and SARS. Cell. 2020;182:722-733.e11.

56. Valdes-Balbin Y, Santana-Mederos D, Quintero L, Fernández S, Rodriguez L, Sanchez Ramirez B, et al. SARS-CoV-2 RBD-Tetanus Toxoid Conjugate Vaccine Induces a Strong Neutralizing Immunity in Preclinical Studies. ACS Chem Biol. 2021;16:1223–33.

57. Song JY, Choi WS, Heo JY, Lee JS, Jung DS, Kim S-W, et al. Safety and immunogenicity of a SARS-CoV-2 recombinant protein nanoparticle vaccine (GBP510) adjuvanted with AS03: A randomised, placebo-controlled, observer-blinded phase 1/2 trial. eClinicalMedicine. 2022;51:101569.

58. Correia-Pinto JF, Csaba N, Alonso MJ. Vaccine delivery carriers: Insights and future perspectives. International Journal of Pharmaceutics. 2013;440:27–38.

59. Mohammadpour R, Yazdimamaghani M, Cheney DL, Jedrzkiewicz J, Ghandehari H. Subchronic toxicity of silica nanoparticles as a function of size and porosity. Journal of Controlled Release. 2019;304:216–32.

60. Kim S-H, Lee, Kim, Lee, Kwon TK, Yun H, et al. The comparative immunotoxicity of mesoporous silica nanoparticles and colloidal silica nanoparticles in mice. IJN. 2013;147.

61. An M, Li M, Xi J, Liu H. Silica Nanoparticle as a Lymph Node Targeting Platform for Vaccine Delivery. ACS Appl Mater Interfaces. 2017;9:23466–75.

62. Reddy ST, Berk DA, Jain RK, Swartz MA. A sensitive in vivo model for quantifying interstitial convective transport of injected macromolecules and nanoparticles. Journal of Applied Physiology. 2006;101:1162–9.

63. Oussoren C, Zuidema J, Crommelin DJA, Storm G. Lymphatic uptake and biodistribution of liposomes after subcutaneous injection. Biochimica et Biophysica Acta (BBA) - Biomembranes. 1997;1328:261–72.

64. Swartz MA, Hubbell JA, Reddy ST. Lymphatic drainage function and its immunological implications: From dendritic cell homing to vaccine design. Seminars in Immunology. 2008;20:147–56.

65. Pal I, Ramsey JD. The role of the lymphatic system in vaccine trafficking and immune response. Advanced Drug Delivery Reviews. 2011;63:909–22.

66. Reddy ST, Rehor A, Schmoekel HG, Hubbell JA, Swartz MA. In vivo targeting of dendritic cells in lymph nodes with poly(propylene sulfide) nanoparticles. Journal of Controlled Release. 2006;112:26–34.

67. Ravasco JMJM, Faustino H, Trindade A, Gois PMP. Bioconjugation with Maleimides: A Useful Tool for Chemical Biology. Chem Eur J. 2019;25:43–59.

68. Kim Y, Ho SO, Gassman NR, Korlann Y, Landorf EV, Collart FR, et al. Efficient Site-Specific Labeling of Proteins via Cysteines. Bioconjugate Chem. 2008;19:786–91.

69. Szijj PA, Bahou C, Chudasama V. Minireview: Addressing the retro-Michael instability of maleimide bioconjugates. Drug Discovery Today: Technologies. 2018;30:27–34.

70. Kaech SM, Wherry EJ, Ahmed R. Effector and memory T-cell differentiation: implications for vaccine development. Nat Rev Immunol. 2002;2:251–62.

71. Jia J, Zhang Y, Xin Y, Jiang C, Yan B, Zhai S. Interactions Between Nanoparticles and Dendritic Cells: From the Perspective of Cancer Immunotherapy. Front Oncol. 2018;8:404.

72. Mata-Haro V, Cekic C, Martin M, Chilton PM, Casella CR, Mitchell TC. The Vaccine Adjuvant Monophosphoryl Lipid A as a TRIF-Biased Agonist of TLR4. Science. 2007;316:1628–32.

73. Casella CR, Mitchell TC. Putting endotoxin to work for us: Monophosphoryl lipid A as a safe and effective vaccine adjuvant. Cell Mol Life Sci. 2008;65:3231–40.

74. Han Q, Bagheri N, Bradshaw EM, Hafler DA, Lauffenburger DA, Love JC. Polyfunctional responses by human T cells result from sequential release of cytokines. Proc Natl Acad Sci USA. 2012;109:1607–12.

75. Lin L, Finak G, Ushey K, Seshadri C, Hawn TR, Frahm N, et al. COMPASS identifies T-cell subsets correlated with clinical outcomes. Nat Biotechnol. 2015;33:610–6.

76. Oberhardt V, Luxenburger H, Kemming J, Schulien I, Ciminski K, Giese S, et al. Rapid and stable mobilization of CD8+ T cells by SARS-CoV-2 mRNA vaccine. Nature. 2021;597:268–73.

77. Kalimuddin S, Tham CYL, Qui M, De Alwis R, Sim JXY, Lim JME, et al. Early T cell and binding antibody responses are associated with COVID-19 RNA vaccine efficacy onset. Med. 2021;2:682-688.e4.

78. Rha M-S, Shin E-C. Activation or exhaustion of CD8+ T cells in patients with COVID-19. Cell Mol Immunol. 2021;18:2325–33.

79. Reinhardt RL, Liang H-E, Locksley RM. Cytokine-secreting follicular T cells shape the antibody repertoire. Nat Immunol. 2009;10:385–93.

80. Feng S, Phillips DJ, White T, Sayal H, Aley PK, Bibi S, et al. Correlates of protection against symptomatic and asymptomatic SARS-CoV-2 infection. Nat Med. 2021;27:2032–40.

81. Khoury DS, Cromer D, Reynaldi A, Schlub TE, Wheatley AK, Juno JA, et al. Neutralizing antibody levels are highly predictive of immune protection from symptomatic SARS-CoV-2 infection. Nat Med. 2021;27:1205–11.

82. Sahin U, Muik A, Derhovanessian E, Vogler I, Kranz LM, Vormehr M, et al. COVID-19 vaccine BNT162b1 elicits human antibody and TH1 T cell responses. Nature. 2020;586:594–9.